TRANSONIC FLOW PAST CONE-CYLINDERS

Thesis by

George E. Solomon

In Partial Fulfillment of the Requirements

For the Degree of

Doctor of Philosophy

California Institute of Technology

Pasadena, California

1953

ACKNOWLEDGMENTS

The author would like to express his appreciation to Drs. H. W. Liepmann, J. D. Cole, and A. Roshko for their helpful advice and constructive criticism throughout the course of the research reported in this thesis. W. W. Willmarth and K. Krishnamurty of the Transonic Research Group contributed to the conduct of the experiments. Mrs. J. Cottingham prepared the report and figures for publication, for which the author is duly grateful.

ABSTRACT

Experimental results are presented for transonic flow past cone-cylinder, axially symmetric bodies. The drag coefficient, surface Mach number, etc. are studied as the free stream Mach number is varied and, wherever possible, the experimental results are compared with theoretical predictions. Interferometric results for several typical flow configurations are shown and an example of shock-free supersonic to subsonic compression is experimentally demonstrated.

The theoretical problem of transonic flow past finite cones is discussed briefly and an approximate solution of the axially symmetric transonic equations, valid for a semi-infinite cone, is presented.

TABLE OF CONTENTS

SYMBOLS

a^*	velocity of sound for $M_\infty = 1.00$
c	chord of the cone
C_D	cone drag coefficient, reference area is the cone base area
C_D^*	drag coefficient at $M_\infty = 1.00$
C_p	pressure coefficient = $\frac{2}{\gamma M_\infty^2}\left[\frac{p_s}{p_\infty} - 1\right]$
C_p^*	pressure coefficient at $M_\infty = 1.00$
d	cone base diameter
K	Gladstone-Dale constant
M_∞	free stream Mach number
M_s	cone surface Mach number
n	index of refraction of air
p_∞	free stream static pressure
p_o	stagnation pressure
p_s	surface static pressure
S	interferometric fringe shift
u	non-dimensional transonic axial-velocity perturbation
v	non-dimensional transonic radial-velocity perturbation
x	axial distance downstream of the cone tip
β_{W_N}	shock wave angle at the cone tip
γ	ratio of specific heats of air = 1.400
δ	axial distance from the cone shoulder to the shock wave
θ	cone semi-angle
ρ	density of air

I. INTRODUCTION

Transonic flow past certain two-dimensional bodies has been the subject of several recent papers and the phenomena are well understood. The theoretical results of Cole (Ref. 1), Guderley and Yoshihara (Ref. 2), Vincenti and Wagoner (Ref. 3), and others apply to two-dimensional symmetrical double wedge airfoils. The experimental results of Bryson (Ref. 4), and Griffith (Ref. 5) substantiate the theoretical work in a very satisfactory manner. More recently, Vincenti and Wagoner (Ref. 6), and Guderley and Yoshihara (Ref. 7) have analyzed the transonic flow past two-dimensional unsymmetrical sections, that is, lifting double wedge airfoils. Current experiments on lifting double wedge airfoils (Ref. 8) at GALCIT indicate that agreement between theoretical and experimental results will again be obtained.

Two-dimensional and axially symmetric transonic flow are of considerable theoretical and practical interest since these two specialized problems are limiting cases of the more complex problem of the flow about an arbitrary three-dimensional body.

The study of axially symmetric transonic flow is not as complete as that of two-dimensional flow. In recent years several papers, notably those of von Kármán (Ref. 9), and Oswatitsch and Berndt (Ref. 10), have studied the similarity rules of axially symmetric transonic flow. Also, Yoshihara (Ref. 11) has calculated the flow about a finite cone at a free stream Mach number of one by a relaxation technique, and has obtained some experimental verification of the theoretical result.

The hodograph problem for general transonic flow past finite cones is discussed in Ref. (8). However, theoretical solutions or experimental results for the complete transonic regime are not, at present, available. This report presents the results of an experimental investigation of the transonic flow past cone-cylinder bodies. A conical tip, followed by a cylindrical afterbody, was chosen as the experimental model for two primary reasons. (1) The relatively simple geometry of a cone-cylinder body may simplify the theoretical problem. (2) Viscous effects are minimized; that is, the boundary layer on the cone surface is in a region of decreasing or constant pressure gradient so that the presence of the boundary layer will not greatly alter the shape of the body forward of the cone shoulder.

Theoretical results for the supersonic flow past a cone were first presented in 1929 by Busemann (Ref. 12). Busemann's solution postulates a semi-infinite cone and assumes that the flow is conical, that is, along rays through the apex of the semi-infinite cone, the flow parameters such as pressure, velocity, etc. being constant. The solution is found by a geometrical construction in the hodograph plane and it is readily apparent that a conical solution exists only so long as a shock wave is attached to the cone apex and, therefore, the free stream Mach number is supersonic. It is interesting to note that Busemann's solution predicts smooth shock-free compression from supersonic to subsonic flow for particular combinations of cone angle and free stream Mach number. The conical solution also shows that for a given cone angle and free stream Mach number, M_∞, the surface Mach number is always less than the Mach number immediately behind

the conical shock wave; as M_∞ decreases, the surface Mach number decreases and eventually passes from supersonic to subsonic values. As was mentioned by Busemann, the conical solution for a semi-infinite cone is completely valid for a finite cone so long as the flow is everywhere supersonic, but when the surface Mach number is less than sonic, the perturbation due to the corner or shoulder of the finite cone is propagated forward through the subsonic portion of the field destroying the conicity of the flow. Thus, the Busemann solution is completely valid for a finite cone only so long as M_∞ is large enough so that the surface Mach number is greater than sonic.

Taylor and Maccoll (Ref. 13) in 1933 presented the results of a numerical integration of the axially symmetric equations of motion for conical flow about semi-infinite cones and also presented experimental verification of their theoretical results. Further experimental verification by Maccoll (Ref. 14) was published in 1937. Both of the above papers noted that deviations of the experiments from the theoretical predictions, notably in the shape of the shock wave, are apparent when the surface Mach number is subsonic.

As was mentioned previously, Yoshihara (Ref. 11) has computed, by relaxation methods, the flow about a cone-cylinder at $M_\infty = 1.00$ and has experimentally verified the calculation. However, theoretical solutions do not exist for the complete transonic regime. Solutions have not been developed for the flow past a finite cone when M_∞ is subsonic or when M_∞ is between sonic and the value of M_∞ at which Busemann's conical solution becomes valid. Drougge (Ref. 15) has computed the flow field between a detached shock wave and a finite

cone by relaxation methods; however, the position and shape of the detached shock wave was determined initially from schlieren photographs.

The experimental results reported in this paper cover several interesting features of the transonic flow about finite cones. The deviations of the surface Mach number from the values predicted by conical theory are examined for values of M_∞ such that the flow field is transonic in nature. The behavior of the surface Mach number for subsonic values of M_∞, and as M_∞ approaches sonic from subsonic values, is examined in some detail so that an extrapolation to $M_\infty = 1.00$ may be made. The above surface Mach number data lead naturally to the evaluation of the drag coefficient, and experimental values of the drag coefficient in the transonic regime are presented.

The physical location of the sonic line in a meridianal plane of the flow about a finite cone is of considerable interest for a theoretical study of the problem of axially symmetric flow. With this fact in mind, an interferometric analysis was made at several typical values of M_∞ so as to determine the local Mach number fields about finite cones. Several examples of supersonic to subsonic, shock-free compression are experimentally demonstrated.

Experimental values of the shock wave angle at the cone tip, particularly at values of M_∞ where the flow field between the shock wave and the cone surface is transonic or subsonic in nature, are presented and a comparison with the values from conical theory is shown.

The conical solution for flow about a semi-infinite cone demonstrates that a conical solution does not exist if, for a given cone angle, M_∞ decreases below a certain minimum M_∞. This minimum M_∞ is

defined to be the M_∞ for which shock wave detachment occurs for a semi-infinite cone. Whether or not the shock wave detachment Mach number for a finite cone can be determined from conical theory is of considerable theoretical interest. Experimental values of the detachment distance of a shock wave from a finite cone tip, the distance obviously being zero at attachment, have been collected from several sources and the results analyzed in this report.

The transonic equations of motion, and boundary conditions as derived by von Kármán (Ref. 9) for axially symmetric flow, require several assumptions as to the relative magnitude of various terms in the exact equations of motion and the related boundary conditions. To demonstrate that the transonic equations retain the important features of the exact equations, an approximate solution of the problem of conical flow about a semi-infinite cone has been developed employing the transonic equations and boundary conditions. A comparison of the exact Busemann solution and the approximate transonic solution is presented in the report.

The author of this report wishes to express his appreciation for their helpful advice and criticism to Drs. H. W. Liepmann, J. D. Cole, and A. Roshko of the California Institute of Technology. The investigation was conducted under the sponsorship of the National Advisory Committee for Aeronautics.

II. EXPERIMENTAL EQUIPMENT

1. Wind Tunnel

The Transonic Wind Tunnel at GALCIT is a continuous flow wind tunnel. For supersonic testing, the test section Mach number may be continuously varied over a wide range by altering the shape of one flexible wall. The test section Mach number is varied by changing the area of a sonic throat downstream of the test section when subsonic tests are being performed. The test section width is 4 inches and the height is 9 inches. The design of the flexible test section wall is discussed in Ref. (16).

2. Interferometer

The interferometer used in the present investigation is of the Mach-Zehnder type. Both light paths of the interferometer are passed through the wind tunnel test section, one beam passing through the flow region under analysis and the other beam passing through the undisturbed flow in the test section upstream of the model. The fringe shifts due to density variations in the boundary layer are eliminated since both beams pass through the boundary layer on the test section walls and are affected almost equally. The growth of the boundary layer between the two beams is not compensated by the above arrangement but the effect is of secondary importance. A detailed description of the GALCIT interferometer and a very complete bibliography on interferometer construction is given in Ref. (17).

3. Models

The models were conical-tipped brass cylinders of 20°, 25°, and 30° semi-angle. The base diameters were between 0.30 inches and 0.50 inches. Thus, the Reynolds numbers for the tests, with the base diameter of the models as the reference dimension, varied from 55,000 to 143,000. The tips of the cones were made as sharp as possible and the maximum tip diameter of the dullest of the models was approximately 1/3 percent of its base diameter. Also, the models were black-nickel plated to improve the photographic definition. The angle of attack and angle of yaw were adjusted to zero by equalizing the pressure on the cone surface at four annular points.

III. EXPERIMENTAL TECHNIQUES

1. Interferometry

An experimental investigation of flow phenomena is facilitated by the employment of an interferometer to determine the density fields in gaseous (or liquid) flows. The interferometer technique possesses the obvious advantage of eliminating the need for placing any type of probe into a flow region where the presence of the probe may completely alter the undisturbed flow field. A disadvantage is also present however, since the values of density are not immediately available as the test is in progress. A more serious disadvantage is the fact that the interferometer integrates the density values on its light paths (see Appendix A) and, thus, the measurement of density is not localized but is influenced by inhomogeneities in the flow which may be well removed from the points of interest.

Two general types of flow are amenable to interferometric analysis, namely two-dimensional and axially symmetric flow. This paper is concerned solely with axially symmetric flow analysis. A discussion of the method employed to reduce the finite fringe interferograms, such as Fig. 2, to density distributions may be found in Appendix A. The method is essentially that outlined in Ref. (18). An excellent discussion of axially symmetric data reduction is given in Ref. (19) where several references to earlier papers in the field will be found.

These earlier papers are mainly concerned with evaluating the interferometer data reduction techniques for axially symmetric flow by investigating the flow about cone-cylinders at Mach numbers and

cone angles where the Busemann conical solution was known to be valid. Ref. (20) presents some experimental results in the same general flow regimes as are investigated in this report.

2. Sonic Line Location by Wave Reflection

The location of the sonic line in a meridianal plane of an axially symmetric transonic flow can be determined experimentally by at least three distinct methods. The first method is by static pressure measurements, the second is by interferometric analysis, and the third method is that of Mach wave reflection from the sonic line. It should be noted, that at the point of reflection, the Mach wave will be perpendicular to the streamline direction through the sonic line.

To locate the sonic line within the flow about a cone, a small-diameter probe was placed in the free stream flow outside of the cone shock wave. The probe was in a position such that the probe shock wave pierced the cone shock wave and entered the flow field about the cone. The shock waves formed by the probe closely approximate Mach waves at large distances from the probe and a typical wave reflection is shown in Fig. 5. The perturbations in the flow about the cone caused by the waves do not appreciably affect the position of the sonic line as shown by Fig. 11 where a comparison is made of the location of the sonic line as found by interferometric analysis and by the wave reflection method. The probe method is much more convenient than the pressure measurement or interferometric method since the phenomenon may be observed with a schlieren system, so that the result is obtained visually.

3. Pressure Measurements

The pressure measurements in this investigation were made either on a micromanometer (accuracy = $\pm$ 0.01 mm. Hg) or on a nomograph Mach meter (Ref. 21).

IV. EXPERIMENTAL RESULTS AND DISCUSSION

1. General Flow Characteristics

An analysis of the flow of a compressible fluid about an axially symmetric finite cone, that is, a cone-cylinder, indicates that five distinct regimes of flow are possible. These regimes are:

I. Subsonic flow at infinity with a region of locally supersonic flow downstream of the cone shoulder. A schlieren photograph of this type of flow is shown in Fig. 1. It should be noted that an extremely weak shock wave originates at the cone shoulder and terminates at the downstream "normal" shock wave. The forked appearance of the base of the terminating "normal" shock wave is an illusion caused by the axial symmetry of the flow. The light rays which pass near the surface of the body, in the region of the rearward branch of the "fork", also pass through the outer portion of the shock and the spurious rearward branch is caused by the light ray deflections in the outer portion of the shock wave. A meridianal section of the shock wave actually includes only the front branch of the fork.

II. Supersonic flow at infinity with a detached shock wave and subsonic flow between the shock wave and the cone. Fig. 2 is a finite fringe interferogram of this type of flow.

III. Supersonic flow at infinity with an attached curved shock wave and subsonic flow between the initial portion of the shock wave and the cone. A schlieren photograph of this

flow is shown in Fig. 3. Taylor and Maccoll's original paper on conical flows (Ref. 13) includes a schlieren photograph of an attached curved shock.

IV. Supersonic flow at infinity with an attached shock wave and mixed supersonic and subsonic flow between the shock wave and the cone. A schlieren photograph of this flow is shown in Fig. 4.

V. Supersonic flow at infinity with completely supersonic flow between the attached shock wave and the cone surface. The Busemann solution applies in this regime and has been verified experimentally in Refs. 13, 14, 19, and 22.

2. Local Mach Number Contours

The local Mach number contours in a meridianal plane for the flow about a 25° semi-angle cone are shown in Figs. 6, 7, 8, and 9 for flow Regimes II, III, and IV. The local Mach number contours for a 30° semi-angle cone in Regime II are shown in Fig. 10. These data were obtained by interferometric analysis as discussed in Appendix A.

The local Mach number contours should be normal to the cone surface since the cone surface is a flat boundary and any pressure gradient at the surface must be parallel to the flat surface. However, near the shoulder of the cone-cylinder, the surface is curved by the effect of the corner expansion on the boundary layer, and thus the local Mach number contours are not quite perpendicular to the cone surface immediately ahead of the shoulder.

3. Sonic Line Location

The location of the sonic line can be determined by interferometric analysis but a more useful method, in the present investigation, was the wave reflection method. The location of the sonic line in Regimes II, III, and IV is discussed below.

Regime II - Examples of the sonic line location in this regime are shown in Figs. 6 and 7. The sonic line originates at the cone shoulder and terminates on the detached shock wave. In Fig. 10, it may be seen that a region of supersonic to subsonic compression exists on the outer portion of the sonic line. The sonic line actually originates slightly upstream of the cone shoulder. This effect is due to the rounding of the cone shoulder by the surface boundary layer.

Regime III - Fig. 8 illustrates the case of the flow with a nearly attached curved shock wave. Again, a small region of supersonic to subsonic compression is present on the outer portion of the sonic line. The free stream Mach number is slightly less than the detachment M_∞ predicted by the exact conical theory. The question of experimental detachment Mach number is discussed below.

Regime IV - Several examples of the sonic line location in this regime are shown on Figs. 9, 11, and 12. Fig. 11 shows the location as determined by interferometric means and as determined by wave reflection. The sonic line again originates at the corner and now terminates at the cone tip and not on the shock wave as in Regimes II and III. A shock-free supersonic to subsonic compression occurs on the forward portion of the sonic line. The location of the sonic line for a

20° semi-angle cone is shown on Fig. 12. The agreement between the theoretical and experimental location is satisfactory near the tip of the cone and for some distance downstream of the tip.*

The question of smooth shock-free supersonic to subsonic compression has been the subject of much discussion in recent years. The above experimental results demonstrate that such a flow is possible. However, the smooth compression is not of primary importance, but rather the conditions under which it occurs. These conditions are that the sonic surface bounds a zone of subsonic flow completely enclosed by a region of supersonic flow and a solid surface.

As an example of non-shock-free supersonic to subsonic compression, consider the flow past a two-dimensional airfoil at high subsonic speeds. The local supersonic zone on the airfoil is terminated by a shock wave and smooth compression through sonic velocity does not occur. In the two-dimensional case, however, the supersonic zone is bounded by a subsonic region and a solid surface. This is the opposite arrangement to that in the flow about a cone, in Regime IV, where shock-free supersonic to subsonic compression does occur.

The above considerations illustrate that the existence (or stability) of shock-free compression through sonic velocity may not be a local phenomenon but may depend on the arrangement of the complete flow field.

---

*The existence of this type of flow is indicated by the experimental results of Taylor and Maccoll (Refs. 13 and 14) and was also discussed by Tsien (Ref. 23).

4. Shock Wave Angle

The angle of the attached shock wave at the nose of the cone was determined for a 20° and a 25° semi-angle cone in flow Regimes III, IV, and V. The values are shown on Fig. 13. Similar experiments are reported in Refs. 13 and 14. Ref. 22 presents data for one cone angle at one Mach number in Regime III and one Mach number in Regime IV. The agreement between the exact theory and the experimental values at the cone tip is very good even in Regimes III and IV where the exact theory is not applicable for the complete finite cone.

5. Surface Mach Number Distribution

The distribution of the surface Mach number, M_s, on a 25° semi-angle cone for various M_∞ is shown on Fig. 14 and that of a 20° semi-angle cone on Fig. 15. Several characteristics of these distributions are of particular interest.

1. M_s near the shoulder deviates from the Busemann conical values as soon as $M_s = 1.00$ is attained. M_s near the cone tip agrees quite well with the conical values until the theoretical detachment M_∞ occurs. M_s at the corner should, except for boundary layer effects, always be sonic if M_s forward of the shoulder is subsonic.

2. As M_∞ approaches 1.00 from the subsonic or from the supersonic regimes, M_s at a particular chordwise station approaches a constant value. This behavior implies that

$$\left.\frac{dM_s}{dM_\infty}\right|_{M_\infty = 1.00} = 0$$

The same behavior of M_s on two-dimensional sections was noted in Ref.(24), and thus the concept of stationary values of M_s at $M_\infty \doteq 1.00$ is established for two-dimensional and axially symmetric flow. Since these two cases represent limiting cases of the flow about general three-dimensional bodies, the stationary M_s concept can probably be applied quite generally if suitable care is taken in choosing the range of M_∞, about $M_\infty = 1.00$, in which the so-called "M_s freeze" is applicable.

3. As M_∞ progresses from a subsonic value, through $M_\infty = 1.00$, and on to a value in Regime V, the M_s at a particular chordwise station probably varies quite smoothly with no abrupt variations, even at attachment of the shock wave, except for a region quite near the tip where large variations may occur when the shock wave attaches.

6. Drag Coefficients

The drag coefficients for the 20° and 25° semi-angle cones are shown on Fig. 16. The values at $M_\infty = 1.00$ were determined by extrapolating the M_s data on Figs. 14 and 15 to $M_\infty = 1.00$.

Using the concept of stationary values of M_s at $M_\infty = 1.00$, the drag curve slope, at $M_\infty = 1.00$, becomes (see Ref. 4 and Appendix C)

$$\left.\frac{dC_D}{dM_\infty}\right|_{M_\infty = 1.00} = \frac{4}{\gamma+1} - \frac{2}{\gamma+1} C_D^* \qquad (1)$$

where C_D^* is the drag coefficient at $M_\infty = 1.00$. The first term, $4/\gamma+1$, of the drag curve slope is derived from the first-order term of the pressure coefficient while the term, $(2/\gamma+1)\, C_D^*$, represents the contribution of the second-order terms. The magnitude of the

second-order term, $(2/\gamma+1)\, C_D^*$, is shown by the difference in slope of the pairs of lines drawn through C_D^* on Fig. 16.

The experimental results also indicate that

$$\left.\frac{d^2 M_s}{dM_\infty^2}\right|_{M_\infty = 1.00} = 0$$

This them implies (see Appendix C) that

$$\left.\frac{d^2 C_D}{dM_\infty^2}\right|_{M_\infty = 1.00} = -\frac{12\gamma + 4}{(\gamma+1)^2} + \frac{10\gamma + 6}{(\gamma+1)^2}\, C_D^*$$

and an estimation can then be made of the range, about $M_\infty = 1.00$, where Eq. (1) is valid.

7. Shock Wave Detachment

Conical flow theory indicates that for a given cone angle of a semi-infinite cone a certain minimum M_∞ is reached below which a conical solution is no longer possible. This value of M_∞ is defined to be the shock wave detachment M_∞. However, a finite cone introduces a characteristic length into the problem so that curved attached shock waves, which would provide the necessary pressure gradient to turn the flow near the cone tip, may exist at M_∞'s less than the conical "detachment" M_∞.

Present experimental results indicate only that shock wave detachment, for a given cone angle, does not occur at an M_∞ greater than that predicted by conical theory. A collection of data from Refs. (22), (25), (26), and (15) is shown on Figs. 17. The ratio, δ/d, where δ is the centerline distance from the shock wave to the plane of the cone shoulder and d is the body diameter at the shoulder, that is, the

sonic point, is seen to approach asymptotically to the value of δ/d at attachment. The asymptotic behavior of δ/d complicates the fairing of the proper curve of δ/d versus M_∞ particularly in view of the paucity of experimental points in the immediate vicinity of shock wave attachment.

In Ref. 27 data are presented for the shock wave detachment distance of several cone angles at $M_\infty = 2.45$. A discrepancy was found between the experimental and theoretical values of the cone angle at which shock wave detachment occurs for a fixed M_∞, detachment appearing to occur at a cone angle slightly greater than that predicted by the conical theory. This behavior would correspond to shock wave detachment, for a fixed cone angle, occurring at an M_∞ less than the theoretical conical value of M_∞. Again, however, the discrepancy may be caused by the manner in which the experimental curve was faired.

Thus, the experimental results appear to indicate only that shock wave detachment for a finite cone occurs at an M_∞ either less than or equal to the value of M_∞ predicted by conical theory but not at a larger M_∞. The fact that shock wave detachment does not appear to occur at an M_∞ greater than that predicted by the conical theory indicates that the presence of a boundary layer on the cone tip does not affect the conicity of the flow near the cone tip to the extent of precipitating detachment of the shock wave.

Fig. 17 also indicates that when the shock wave detachment distance is large, the position of the shock wave is dependent only on the diameter of the cone at the shoulder or sonic point and is independent

of the cone angle. When the shock wave is quite near the cone tip, however, the detachment distance is also dependent on the cone angle. This manner of behavior of the shock wave separation distance was discussed by Busemann (Ref. 28) and shown experimentally for two-dimensional wedge sections by Griffith (Ref. 29).

8. Transonic Similarity

The transonic similarity rules for the drag coefficient and pressure coefficient, as derived in Ref. (10), cannot be checked by the experimental results of this report. The derivation assumes that the cone surface boundary condition is the approximate tangency condition which is valid for relatively small angles. A 20° semi-angle cone is the minimum angle cone for which detached shock wave flow can be obtained in the Transonic Wind Tunnel, and thus, the experimental models were 20°, 25°, and 30° semi-angle cones. The experimental cone-angles are much larger than the cone angles for which the approximate tangency condition is reasonable, and, therefore the transonic similarity rules of Ref. (10) are not applicable.

V. THEORETICAL CONSIDERATIONS

At the present time, theoretical solutions have not been found to describe the flow about a finite cone for the complete Mach number range. Theoretical solutions are available for only two Mach number regimes, namely;

1. Exact conical theory may be applied if the surface Mach number is greater than sonic.
2. At $M_\infty = 1.00$, Yoshihara (Ref. 11) has calculated the flow about small angle cones by a relaxation technique.

No solution has been determined if M_∞ is less than sonic. However, Van Dyke's second order supersonic theory and technique (Ref. 30) possibly can be applied to the subsonic case since, if the appropriate changes of sign are made in the particular solution found by Van Dyke for the supersonic case, the particular solution becomes valid for the subsonic case.

A solution remains to be found for the regime between $M_\infty = 1.00$ and the value of M_∞ where M_s becomes equal to 1.00. The problem would be greatly simplified if the transonic equations could be employed. To test the feasibility of the approximations inherent in the transonic equations, an approximate solution has been found for conical flow about a semi-infinite cone using the transonic equations. The details of the solution are presented in Appendix B.

The solution is compared with the exact conical theory in Figs. 18 and 19. Fig. 18 shows the comparison between the shock wave angles predicted by the exact theory and by the transonic approximation. The

surface Mach number comparison is shown on Fig. 19. From Fig. 19 it can be seen that the transonic approximation is quite satisfactory and is probably better than slender-body cone theory, since slender-body cone theory does not consider the presence of the conical shock wave. Also, Figs. 18 and 19 show the agreement of the cone angle at shock wave detachment as found from the transonic solution and from the exact theory.

The above comparison of the exact conical solution and the approximate solution indicates that the transonic equations contain all the terms of importance in the exact equations for conical flow about cones, so that the transonic equations may be employed with confidence in the range of M_∞ from $M_\infty = 1.00$ to an M_∞ for which $M_s = 1.00$.

VI. CONCLUSIONS

The variation of drag coefficient with M_∞ was determined experimentally. The slope of C_D versus M_∞ at $M_\infty = 1.00$ agrees with the theoretical prediction. The deviation of C_D versus M_∞, from the conical flow value of C_D, when $M_s < 1.00$ is demonstrated.

The experimental results for the shock wave angle, sonic line location, and surface Mach number in the region near the cone tip, indicate that the flow is conical near the tip of a finite cone even when the surface Mach number is less than sonic. The surface Mach numbers for the rest of the cone deviate from the exact conical values when $M_s < 1.00$. Also, a case of shock-free supersonic to subsonic compression is demonstrated experimentally.

An approximate solution for transonic conical flow has been developed and the agreement with the exact conical theory indicates that the axially symmetric transonic equations retain the important features of the exact equations.

Present experimental values of the detachment distance of a shock wave from a finite cone tip do not demonstrate agreement with the detachment Mach number predicted by conical theory for a semi-infinite cone and the question of shock wave detachment from a finite cone remains undecided.

APPENDIX A

REDUCTION OF INTERFEROMETER DATA

An interferometer determines the advancement or retardation of a light wave in a medium with respect to a coherent light wave in a reference medium. Since the wave velocities are a function of the indices of refraction of the respective media, and consequently of the densities of the media, it may be shown that

$$dS = \frac{K}{\lambda_o} \left[\rho(\ell) - \rho_R \right] d\ell \qquad \text{(A-1)}$$

where

$\rho(\ell)$ = density of the undetermined medium

ρ_R = density of the reference medium

ℓ = path length

K = Gladstone-Dale constant

λ_o = wave length in vacuum of the light employed

S = fringe shift - in the case of finite fringe interferograms, this is the ratio of the displacement of a fringe to the interval between undisturbed fringes

In Eq. (A-1) it has been assumed that the light beams traverse identical geometrical paths, so that refraction, if present, is neglected. Also, the relationship between the index of refraction, n, and density is assumed to be

$$n = 1 + K\rho \qquad \text{(A-2)}$$

If $n = 1 + \alpha$ where $\alpha << 1$, Eq. (A-2)is obtained by linearizing

the Lorentz law.

For the axially symmetric case, the fringe shift for a light path perpendicular to the axis of symmetry becomes

$$S(y) = \frac{2K}{\lambda_o} \int_y^\infty \frac{\left[\rho(r) - \rho_R\right] r\,dr}{\left[r^2 - y^2\right]^{1/2}}$$

where

r = radial distance from the axis of symmetry to a point on the light path

y = perpendicular distance from the axis of symmetry to the light path

In the present investigation, the density field was bounded by a shock wave at a distance, y_S, from the axis and the reference density was the free stream density, ρ_∞, thus

$$S(y) = \frac{2K}{\lambda_o} \int_y^{y_S} \frac{\left[\rho(r) - \rho_\infty\right] r\,dr}{\left[r^2 - y^2\right]^{1/2}} \qquad \text{(A-3)}$$

Weyl (Ref. 31) introduced the assumption that $S(y)$ is a linear function of y^2 in a small interval of y. The validity of this assumption, for the present investigation, is indicated by the parabolic nature of the typical fringe shift curves shown on Fig. 21. If the substitutions

$$v = r^2$$

$$u = y^2$$

$$u_S = y_S^2$$

are made, Eq. (A-3) becomes

$$S(u) = \frac{K}{\lambda_o} \int_u^{u_S} \frac{\left[\rho(v) - \rho_\infty\right] dv}{\sqrt{v - u}} \qquad \text{(A-4)}$$

This is analogous to the solution of Abel's problem. The solution of Eq. (A-4) for ρ is

$$\rho(w) - \rho_\infty = -\frac{\lambda_o}{\pi} \int_w^{u_s} \frac{(dS/du)\, du}{\sqrt{u - w}} \qquad \text{(A-5)}$$

where $w = y^2$. A complete proof of the solution may be found in Ref. (19).

If the region of integration in Eq. (A-5) is divided into equal increments in r of width a, then

$$r_i = ia$$

where i is an integer. A numerical evaluation of Eq. (A-5) is, then,

$$\frac{\rho(r_i)}{\rho_\infty} = 1 + \frac{2\lambda_o}{\pi K a \rho_\infty} \sum_{K=i}^{n-1} (S_K - S_{K+1})\, A_{Ki} \qquad \text{(A-6)}$$

where

$$r_s = Na$$

and

$$A_{Ki} = \frac{\sqrt{(K+1)^2 - i^2} - \sqrt{K^2 - i^2}}{2K+1}$$

The above solution of the problem is essentially that of Ref. (18) and a table of A_{Ki} for fifty intervals will be found in Ref. (18).

From the density ratio determined by Eq. (A-6) the local Mach number may be computed. An approximate correction to the local stagnation pressure, p_o', downstream of the shock wave was made by assuming, that on the cone surface, p_o' was determined by the nose shock wave angle, and at a given chordwise station p_o' varied linearly to the value on the shock wave at the given station. If the approximate streamlines are calculated, as in Ref. (20), a more refined correction is obtained. From the experimental values of the local Mach number, a topographic map was plotted, and from this map the desired Mach number contours are found.

1. Conical Fields

If it is desired to determine whether or not a given axially symmetric field is conical, a simple test can be made. Returning to Eq. (A-3)

$$S(y) = \frac{2K}{\lambda_o} \int_{y}^{y_s} \frac{\left[\rho(r) - \rho_\infty\right] r\,dr}{\left[r^2 - y^2\right]^{1/2}} \qquad \text{(A-7)}$$

it is assumed that

$$\rho = \rho(\eta)$$

where

$\eta = r/x$

x = axial distance from the conical origin

Then Eq. (A-7) becomes

$$\frac{S(y)}{x} = \frac{2K}{\lambda_o} \int_{\eta_1}^{\eta_s} \frac{\left[\rho(\eta) - \rho_\infty\right] \eta\,d\eta}{\left[\eta^2 - \eta_1^2\right]^{1/2}}$$

where

η_s = tangent of the shock wave angle

$\eta_1 = y/x$

Thus, if the field is truly conical,

$$\frac{S(y)}{x} = f\left(\frac{y}{x}\right)$$

and a plot of $S(y)/x$ versus y/x for various values of x will yield a group of coincident curves. Examples of this technique are shown in Refs. (19) and (20). It is interesting to note that in Ref. (20), Fig. 7 indicates conical flow near a cone tip for flow Regime IV, that is, a 35° semi-angle cone at $M_\infty = 1.87$, using the above technique.

2. Subsidiary Considerations

A. Model Size

From Eq. (A-3), it is evident that the fringe shift at a particular chordwise and radial station is a linear function of the model size, for fixed values of density. Thus the model should be as large as is compatible with the test section dimensions with regard to blocking, etc.

B. Finite Fringe Spacing

The fringe spacing in the undisturbed field must be such that a sufficient number of data points may be determined between the shock wave and the cone surface at a particular chordwise station. However, for a given fringe shift, S, the displacement of the fringe is proportional to the undisturbed fringe spacing, and the accuracy of the fringe data will be improved by increasing the undisturbed spacing. A compromise must be effected between the desire for many fringe shift points at a given chordwise station and the accuracy of the individual points. In the present investigation, this compromise precluded a study by interferometry of the flow properties in the immediate vicinity of the cone tip when the shock wave was attached.

C. Accuracy

The accuracy of the interferometric method is affected by refraction, inhomogeneities in the reference flow, the numerical approximation, etc. An estimate of the accuracy can be obtained by noting the comparison of interferometer data and shock reflection data on Fig. 11 and the values of local Mach number behind the shock wave indicated on Figs. 6, 7, 8, 9, and 10.

Comprchcnsivc discussions of the accuracy of the method may be found in Ref. (18) and (19).

APPENDIX B

TRANSONIC APPROXIMATION FOR CONICAL FLOW

In discussing axially symmetric transonic flow, the following approximations to the exact equations and boundary conditions are employed.

If q_1 is the velocity in the axial or x-direction and q_2 is the velocity in the radial or r-direction it is assumed that

$$q_1 = a^* + \phi_x$$

$$q_2 = \phi_r$$

where a^* is the velocity of sound at $M_\infty = 1.00$, ϕ is the perturbation potential and $\phi_x, \phi_r << a^*$. Then, defining

$$u = \frac{\gamma+1}{a^*}\,\phi_x$$

$$v = \frac{\gamma+1}{a^*}\,\phi_r$$

the continuity equation is approximated by

$$u u_x - v_r - \frac{1}{r}\,v = 0 \qquad \text{(B-1)}$$

and the condition of irrotationality becomes

$$u_r - v_x = 0 \qquad \text{(B-2)}$$

The exact tangency condition on the body surface is replaced by

$$v_0 = (\gamma+1)\,\tan\theta \qquad \text{(B-3)}$$

where

v_0 = v on surface of body

θ = inclination angle of body surface

The above relations are derived in greater detail in Ref. (9).

To test the feasibility of the approximations inherent in

Eqs. (B-1), (B-2), and (B-3) an approximate solution for the flow about a semi-infinite cone will be developed. This approximation will then be compared with the Busemann solution of the exact equations.

1. Conical Solution

Assuming that u and v are functions of σ where

$$\sigma = \frac{x}{r}$$

Eqs. (B-1) and (B-2) become

$$u u_\sigma + \sigma v_\sigma - v = 0 \tag{B-1'}$$

$$\sigma u_\sigma + v_\sigma = 0 \tag{B-2'}$$

A solution of the form

$$u = f(v) \tag{B-4}$$

will be sought. From Eq. (B-4)

$$\frac{du}{d\sigma} = \frac{du}{dv}\,\frac{dv}{d\sigma}$$

but from Eq. (B-2')

$$\frac{dv}{d\sigma} = -\sigma\,\frac{du}{d\sigma}$$

Therefore

$$\frac{du}{dv} = -\frac{1}{\sigma} \tag{B-5}$$

This relationship, Eq. (B-5), is exact (see Ref. 32).

Differentiating Eq. (B-5) with respect to σ yields

$$\frac{dv}{d\sigma} = \frac{1}{\sigma^2\,\dfrac{d^2u}{dv^2}} \tag{B-6}$$

and therefore

$$\frac{du}{d\sigma} = -\frac{1}{\sigma^3\,\dfrac{d^2u}{dv^2}} \tag{B-7}$$

Substituting Eqs. (B-5), (B-6), and (B-7) into Eq. (B-1') the result is

$$\nu \frac{d^2u}{d\nu^2} + \frac{du}{d\nu} = u\left(\frac{du}{d\nu}\right)^3 \qquad \text{(B-8)}$$

The following conditions are imposed on Eq. (B-8):

(a) At the Shock Wave

If u_1 and ν_1 are the values of u and ν at the shock wave, then, from the transonic shock polar relation,

$$\nu_1 = (u_\infty - u_1)\sqrt{\frac{u_\infty + u_1}{2}} \qquad \text{(B-1a)}$$

where

$$u_\infty = M_\infty^2 - 1$$

The shock wave angle, β, is given by

$$\cot \beta = \frac{\nu_1}{u_\infty - u_1}$$

hence, from Eq. (B-5)

$$\left.\frac{du}{d\nu}\right|_1 = -\frac{u_\infty - u_1}{\nu_1} \qquad \text{(B-2a)}$$

(b) On the Cone Surface

The tangency condition must be satisfied, hence

$$\nu_0 = (\gamma+1)\tan\theta \qquad \text{(B-1b)}$$

From Eq. (B-5)

$$\left.\frac{du}{d\nu}\right|_0 = -\tan\theta \qquad \text{(B-2b)}$$

where

ν_0 = ν on the cone surface

θ = cone semi-angle

An exact solution of Eq. (B-8) has not been found. However, if the right-hand side of Eq. (B-8) is assumed to be small, an iteration solution may be found.

2. First Approximation

As a first approximation to the solution, set the right-hand side of Eq. (B-8) equal to zero; that is,

$$\frac{d}{dv}\left(v\,\frac{du}{dv}\right) = 0 \tag{B-9}$$

The solution of Eq. (B-9) is

$$u = A \log Bv \tag{B-10}$$

Applying conditions (B-1a) and (B-2a) to this solution, Eq. (B-10) becomes

$$u = u_1 - (u_\infty - u_1) \log \frac{v}{v_1} \tag{B-11}$$

3. Second Approximation

As a second approximation to the solution of Eq. (B-8), the right-hand side of Eq. (B-8) is assumed to be given with sufficient accuracy by Eq. (B-11). Hence

$$\frac{d}{dv}\left(v\,\frac{du}{dv}\right) = -\frac{u_1\,(u_\infty - u_1)^3}{v^3} + \frac{(u_\infty - u_1)^4}{v^3} \log \frac{v}{v_1} \tag{B-12}$$

The solution of Eq. (B-12) is

$$u = \frac{(u_\infty - u_1)^3}{4v^2}\left[-u_1 + (u_\infty - u_1) + (u_\infty - u_1) \log \frac{v}{v_1}\right] + C \log Dv \tag{B-13}$$

Applying conditions (B-1a) and (B-2a) to this solution, Eq. (B-13) becomes

$$u = \frac{(u_\infty - u_1)^3}{4v^2}\left[-u_1 + (u_\infty - u_1) + (u_\infty - u_1) \log \frac{v}{v_1}\right]$$

$$- \frac{(u_\infty + 5u_1)\,(u_\infty - u_1)}{2\,(u_\infty + u_1)} \log \frac{v}{v_1} - \frac{u_\infty\,(u_\infty - 5u_1)}{2\,(u_\infty + u_1)} \tag{B-14}$$

The values of u_1 and v_1 appearing in Eq. (B-14) are not

independent of the cone semi-angle θ . Applying condition (B-2b) to Eq. (B-14) and solving for v_1 , the result is

$$\log v_1 = \log (\gamma+1) \tan\theta + \frac{\left[(\gamma+1)\tan\theta\right]^2 \left[u_\infty + 5u_1\right]}{(u_\infty + u_1)(u_\infty - u_1)^3}$$

$$- \left[\frac{u_1}{u_\infty - u_1} - \frac{1}{2}\right] - \frac{2(\gamma+1)^3 \tan^4\theta}{(u_\infty - u_1)^4} \qquad \text{(B-15)}$$

The transonic shock polar relation also must be satisfied, hence

$$v_1 = (u_\infty - u_1)\sqrt{\frac{u_\infty + u_1}{2}} \qquad \text{(B-16)}$$

Due to the nature of Eq. (B-15), explicit solutions of Eqs. (B-15) and (B-16) for u_1 and v_1 in terms of u_∞ and θ have not been found. However, a solution may be found graphically.

The values of u_1 and v_1 thus determined for a given θ and u_∞ may be introduced into Eq. (B-14). If the value of u on the surface, u_o , is desired, then substitution of

$$v = v_o = (\gamma+1)\tan\theta$$

in Eq. (B-14) yields u_o .

It should be noted that, for a given θ and u_∞ , two sets of values for u_1 and v_1 are found. These correspond to the "strong" and "weak" shock waves.

4. Comparison of the Second Approximation and the Busemann Conical Solution

A. Wave Angle

The wave angle, β , is determined by the values of u_1 and v_1 , since

$$\cot\beta = \frac{v_1}{u_\infty - u_1}$$

The degree of agreement is apparent on Fig. 18.

B. Surface Mach Number

In terms of u_o and v_o, the surface Mach number is

$$M_S^2 = \frac{2}{\gamma+1} A \left[\frac{1}{1 - \frac{\gamma-1}{\gamma+1} A} \right] \qquad \text{(B-17)}$$

where

$$A = \left[1 + \frac{u_o}{\gamma+1} \right]^2 + \left(\frac{v_o}{\gamma+1} \right)^2$$

The usual transonic approximation reduces Eq. (B-17) to

$$M_S^2 = 1 + u_o \qquad \text{(B-18)}$$

Eq. (B-17) is shown on Fig. 19. The agreement with the exact theory is quite satisfactory.

C. Apple Curve

Two sets of values of u_1 and v_1 will satisfy Eqs. (B-15) and (B-16). The two solutions correspond to the "strong" and "weak" shock wave solutions predicted by Busemann. If the values of u_o and v_o for all possible cone angles and for both types of solution are plotted in the hodograph, the resultant curve is Busemann's "apple" curve. The "apple" curve found in the second approximation is shown in Fig. 20.

APPENDIX C

VARIATION OF PRESSURE AND DRAG COEFFICIENTS NEAR $M_\infty = 1.00$

The pressure coefficient

$$C_p = \frac{2}{\gamma M_\infty^2} \left[\frac{p_S}{p_\infty} - 1 \right]$$

where

p_S = surface static pressure

p_∞ = free-stream static pressure

may, in transonic flow, be written as

$$C_p = \frac{2}{\gamma M_\infty^2} \left\{ \left[\frac{1 + \frac{\gamma-1}{2} M_\infty^2}{1 + \frac{\gamma-1}{2} M_S^2} \right]^{\gamma/\gamma-1} - 1 \right\} \qquad \text{(C-1)}$$

where M_S is the surface Mach number. In Eq. (C-1) it has been assumed that

$$\frac{\Delta p_o}{p_o} \sim O\,(M^2-1)^3$$

that is, the stagnation pressure loss across any shock waves may be neglected.

Defining η and ξ as

$$\eta = M_\infty^2$$

$$\xi = M_S^2$$

Eq. (C-1) becomes

$$C_p = f(\eta, \xi) = \frac{2}{\gamma \eta} \left\{ \left[\frac{1 + \frac{\gamma-1}{2} \eta}{1 + \frac{\gamma-1}{2} \xi} \right]^{\gamma/\gamma-1} - 1 \right\} \qquad \text{(C-2)}$$

For a fixed body geometry, M_S is a function of M_∞ only, therefore

$$\xi = \xi(\eta)$$

Thus, the first and second total derivatives of C_p with respect to η are

$$\frac{dC_p}{d\eta} = f_\eta + f_\xi \frac{d\xi}{d\eta} \tag{C-3}$$

and

$$\frac{d^2C_p}{d\eta} = f_{\eta\eta} + 2 f_{\eta\xi} \frac{d\xi}{d\eta} + f_{\xi\xi} \left(\frac{d\xi}{d\eta}\right)^2 + f_\xi \frac{d^2\xi}{d\eta^2} \tag{C-4}$$

In general, $d\xi/d\eta$ and $d^2\xi/d\eta^2$ are not known; however, an argument presented by Liepmann and Bryson (Ref. 24) shows that for $\eta = 1.00$, $d\xi/d\eta = 0$. The same argument, namely that M_S has a stationary value at $M_\infty = 1.00$, cannot be used to evaluate $d^2\xi/d\eta^2$. However, an inspection of the experimental data (see Figs. 14 and 15) indicates that M_S versus M_∞ has an inflection point at $M_\infty = 1.00$ and, thus, $d^2\xi/d\eta^2 = 0$ at $\eta = 1.00$.

Using Eqs. (C-3) and (C-4) and the above argument, the derivatives of C_p become

$$\left(\frac{dC_p}{d\eta}\right)^* = f_\eta^*$$

$$\left(\frac{d^2C_p}{d\eta^2}\right)^* = f_{\eta\eta}^*$$

where $(\ )^*$ indicates evaluation at $\eta = 1.00$, that is, at $M_\infty = 1.00$. The derivatives of C_p with respect to M_∞ are then

$$\left(\frac{dC_p}{dM_\infty}\right)^* = 2 f_\eta^*$$

$$\left(\frac{d^2C_p}{dM_\infty^2}\right)^* = 4 f_{\eta\eta}^* + 2 f_\eta^*$$

The partial derivatives $f_{\eta\eta}$ and f_η may be calculated from Eq. (C-2) and thus

$$\left(\frac{dC_p}{dM_\infty}\right)^* = \frac{4}{\gamma+1} - \frac{2}{\gamma+1} C_p^* \tag{C-5}$$

$$\left(\frac{d^2C_p}{dM_\infty^2}\right)^* = -\frac{12\gamma+4}{(\gamma+1)^2} + \frac{10\gamma+6}{(\gamma+1)^2}\,C_p^* \qquad \text{(C-6)}$$

The fore-drag coefficient of a finite cone is given by

$$C_D = \int_0^1 C_p(\alpha)\,d\alpha$$

where

$$\alpha = \left(\frac{r}{R}\right)^2$$

and

r = local cone radius

R = cone base radius

Using Eqs. (C-5) and (C-6), the derivatives of C_D are

$$\left(\frac{dC_D}{dM_\infty}\right)^* = \frac{4}{\gamma+1} - \frac{2}{\gamma+1}\,C_D^* \qquad \text{(C-7)}$$

and

$$\left(\frac{d^2C_D}{dM_\infty^2}\right)^* = -\frac{12\gamma+4}{(\gamma+1)^2} + \frac{10\gamma+6}{(\gamma+1)^2}\,C_D^* \qquad \text{(C-8)}$$

A comparison of Eq. (C-7) and experimental data is shown on Fig. 16. Eqs. (C-5) and (C-7) were given previously by Bryson (Ref. 4).

It should be noted that the first term, $4/\gamma+1$, of $(dC_p/dM_\infty)^*$ may be derived from the linearized transonic C_p (Ref. 1) which is

$$C_p = 2\,\frac{M_\infty^2 - M_S^2}{(\gamma+1)} \qquad \text{(C-9)}$$

The second term of Eq. (C-5), $-(2/\gamma+1)\,C_p^*$, is then of the nature of a second-order correction term. However, if $(d^2C_p/dM_\infty^2)^*$ is computed from Eq. (C-9), the result does not agree with the first term of Eq. (C-6) and is, in fact, of opposite sign.

REFERENCES

1. Cole, J. D.: Drag of a Finite Wedge at High Subsonic Speeds. Jour. of Math. and Physics, Vol. 30, No. 2, July 1951.

2. Guderley, G. and Yoshihara, H.: The Flow Over a Wedge Profile at Mach Number One. AF Tech. Rept. 5783, July 1949.

3. Vincenti, W. G. and Wagoner, C. B.: Transonic Flow Past a Wedge Profile with Detached Bow Wave - General Analytical Method and Final Calculated Results. NACA T.N. 2339, April 1951.

4. Bryson, A. E., Jr.: An Experimental Investigation of Transonic Flow Past Two-Dimensional Wedge and Circular-Arc Sections Using a Mach-Zehnder Interferometer. NACA T.N. 2560, November 1951.

5. Griffith, W.: Shock-Tube Studies of Transonic Flow Over Wedge Profiles. Jour. Aero. Sci., Vol. 19, No. 4, April 1952.

6. Vincenti, W. G. and Wagoner, C. B.: Theoretical Study of the Transonic Lift of a Double-Wedge Profile with Detached Bow Wave. NACA T.N. 2832, December 1952.

7. Guderley, G. and Yoshihara, H.: Two-Dimensional Unsymmetric Flow Patterns at Mach Number One. AF Tech. Rept. 6683, January 1952.

8. Cole, J. D., Solomon, G. E., and Willmarth, W. W.: Transonic Flow Past Simple Bodies. To be published in the Journal of the Aeronautical Sciences.

9. Kármán, Th. von: The Similarity Law of Transonic Flow. Jour. of Math. and Physics, Vol. 26, No. 3, October 1947.

10. Oswatitsch, K. and Berndt, S. B.: Aerodynamic Similarity at Axisymmetric Transonic Flow Around Slender Bodies. Royal Institute of Technology, Sweden, Aero. TN 15, May 1950.

11. Yoshihara, H.: On the Flow Over a Cone-Cylinder Body at Mach Number One. WADC Tech. Rept. 52-295, November 1952.

12. Busemann, A.: Drücke auf Kegelförmige Spitzen bei Bewegung mit Überschallgeschwindigkeit. Zeit. f. Ang. Math. u. Mech., Vol. 9, No. 6, December 1929.

13. Taylor, G. I. and Maccoll, J. W.: The Air Pressure on a Cone Moving at High Speeds. Proc. Royal Soc. of London, Ser. A, Vol. 139, pp. 278-311, 1933.

14. Maccoll, J. W.: The Conical Shock Wave Formed by a Cone Moving at a High Speed. Proc. Royal Soc. of London, Ser. A, Vol. 159, pp. 459-472, 1937.

15. Drougge, G.: The Flow Around Conical Tips in the Upper Transonic Range. Aero. Res. Inst. of Sweden (Stockholm), Rept. 25, 1948.

16. Dhawan, S. and Roshko, A.: A Flexible Nozzle for a Small Supersonic Wind Tunnel. Jour. Aero. Sci., Vol. 18, No. 4, April 1951.

17. Ashkenas, H. I. and Bryson, A. E.: Design and Performance of a Simple Interferometer for Wind Tunnel Measurements. Jour. Aero. Sci., Vol. 18, No. 2, February 1951.

18. Gooderum, P. B. and Wood, G. P.: Density Fields Around a Sphere at Mach Numbers 1.30 and 1.62. NACA T.N. 2173, August 1950.

19. Bennett, F. D., Carter, W. C., and Bergdolt, V. E.: Interferometric Analysis of Airflow about Projectiles in Free Flight. Jour. Applied Physics, Vol. 23, No. 4, pp. 453-469, April 1952.

20. Bergdolt, V. E.: Air Flow About Cone-Cylinders with Curved Shock Waves. Ballistic Research Laboratories, Rept. No. 832, September 1952.

21. Liepmann, H. W. and Ashkenas, H.: Shock Wave Oscillations in Wind Tunnels. Jour. Aero. Sci., Vol. 14, No. 5, May 1947.

22. Muirhead, V. U.: Flow Field Around a Finite Cone with Shock. A.E. Thesis, Calif. Inst. of Tech., 1949.

23. Tsien, H. S.: The Limiting Line in Mixed Subsonic and Supersonic Flow of Compressible Fluids. NACA T.N. 961, November 1944.

24. Liepmann, H. W. and Bryson, A. E., Jr.: Transonic Flow Past Wedge Sections. Jour. Aero. Sci., Vol. 17, No. 12, December 1950.

25. Marschner, B. W.: An Investigation of Detached Shock Waves. A.E. Thesis, Calif. Inst. of Tech., 1948.

26. Heberle, J. W., Wood, G. P., and Gooderum, P. B.: Data on Shape and Location of Detached Shock Waves on Cones and Spheres. NACA T.N. 2000, January 1950.

27. Johnston, G. W.: An Investigation of the Flow About Cones and Wedges at and Beyond the Critical Angle. Univ. of Toronto Inst. of Aerophysics, Rept. No. 24, December 1952.

28. Busemann, A.: A Review of Analytical Methods for the Treatment of Flows with Detached Shocks. NACA T.N. 1858, April 1949.

29. Griffith, W. C.: Transonic Flow. Dept. of Physics, Princeton University, Tech. Rept. II-7, December 1950.

30. Van Dyke, M. D.: A Study of Second-Order Supersonic-Flow Theory. NACA T.N. 2200, January 1951.

31. Weyl, F. J.: Naval Ordnance Report 211-45, December 1945.

32. Ferri, A.: Elements of Aerodynamics of Supersonic Flows. The Macmillan Company, New York, 1949.

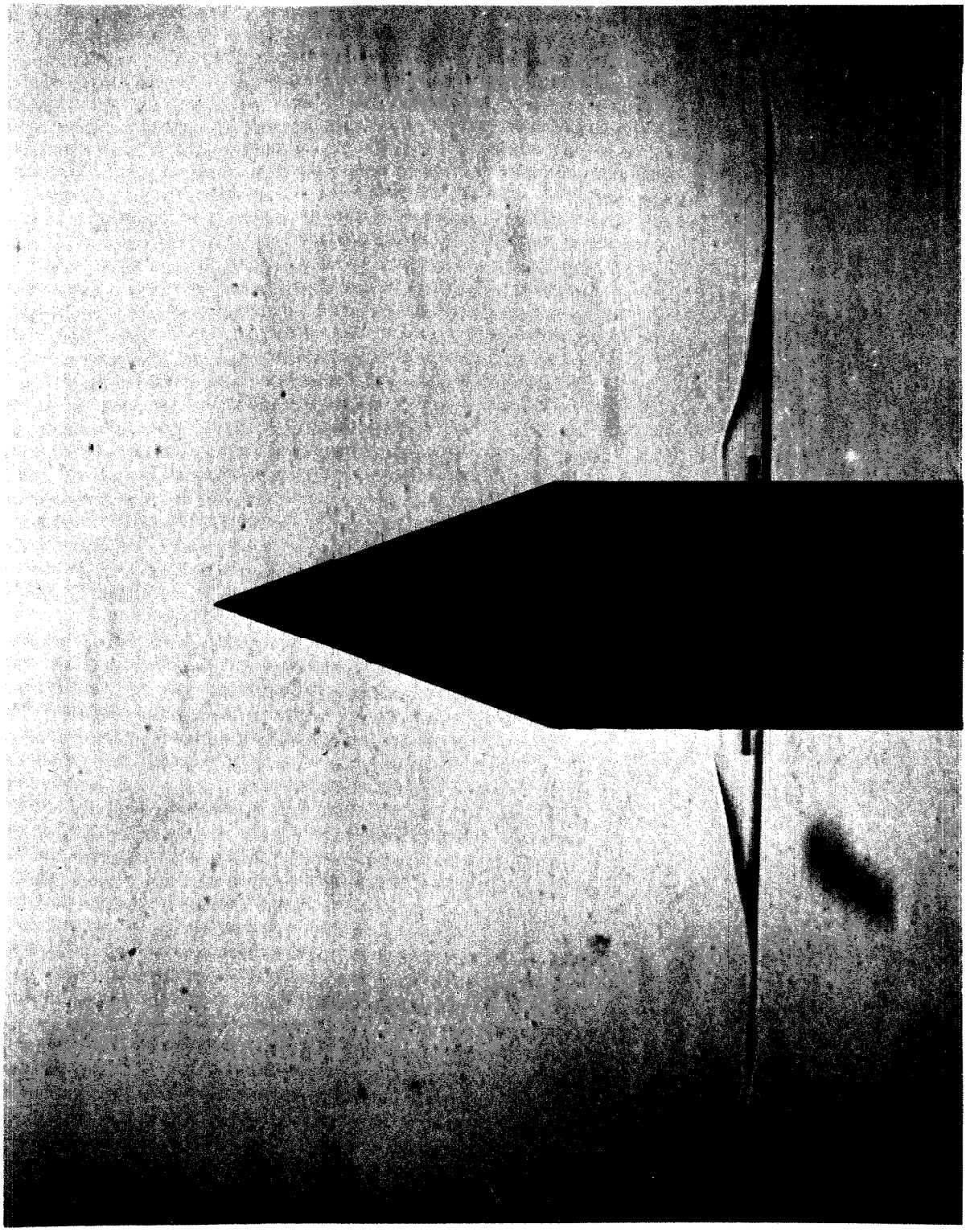

20° SEMI-ANGLE CONE-CYLINDER
$M_\infty = 0.942$
FIG. 1

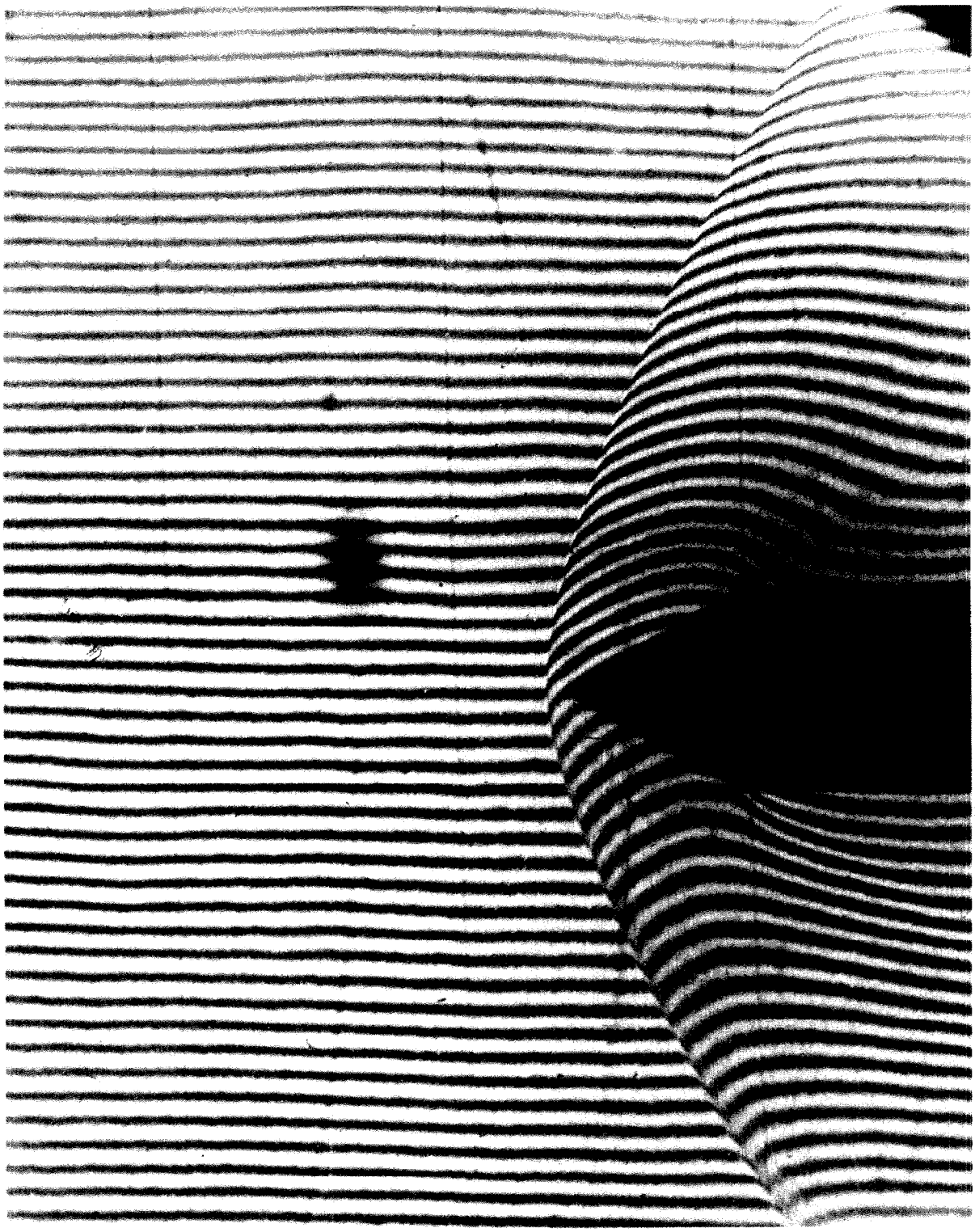

FINITE FRINGE INTERFEROGRAM
30° SEMI-ANGLE CONE-CYLINDER
$M_\infty = 1.280$

FIG. 2

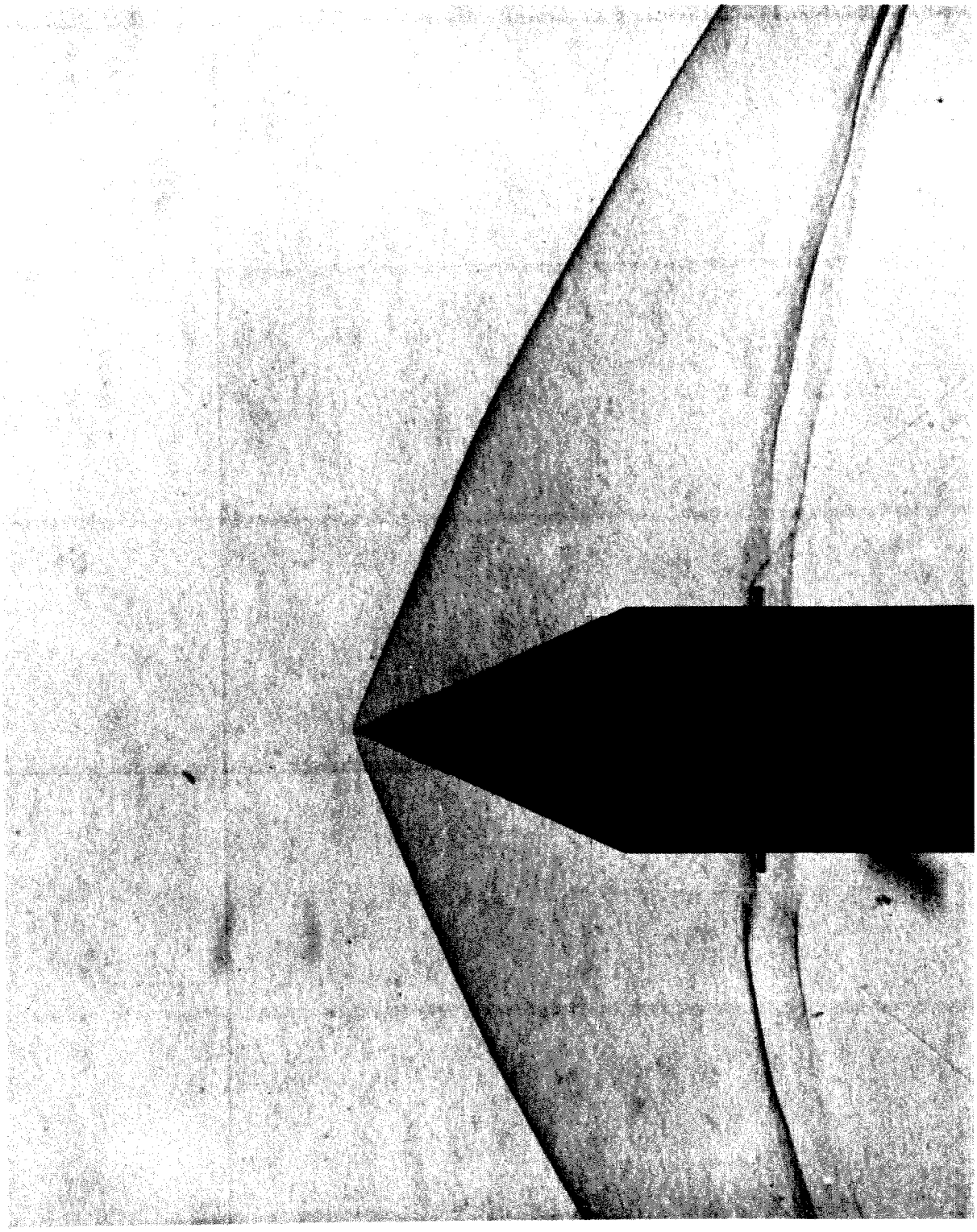

25° SEMI-ANGLE CONE-CYLINDER
$M_\infty = 1.328$
FIG. 3

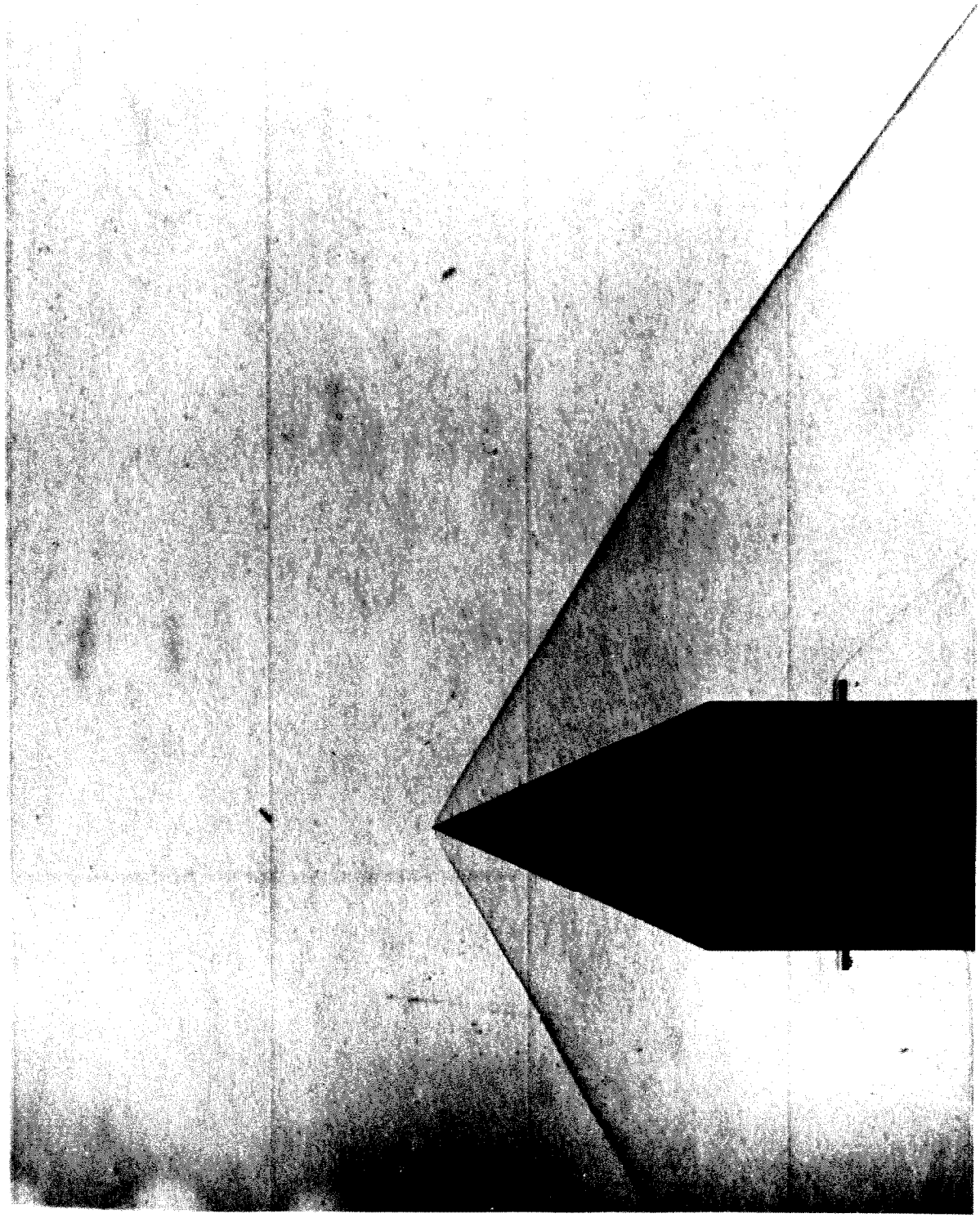

25° SEMI-ANGLE CONE-CYLINDER
$M_\infty = 1.415$

FIG. 4

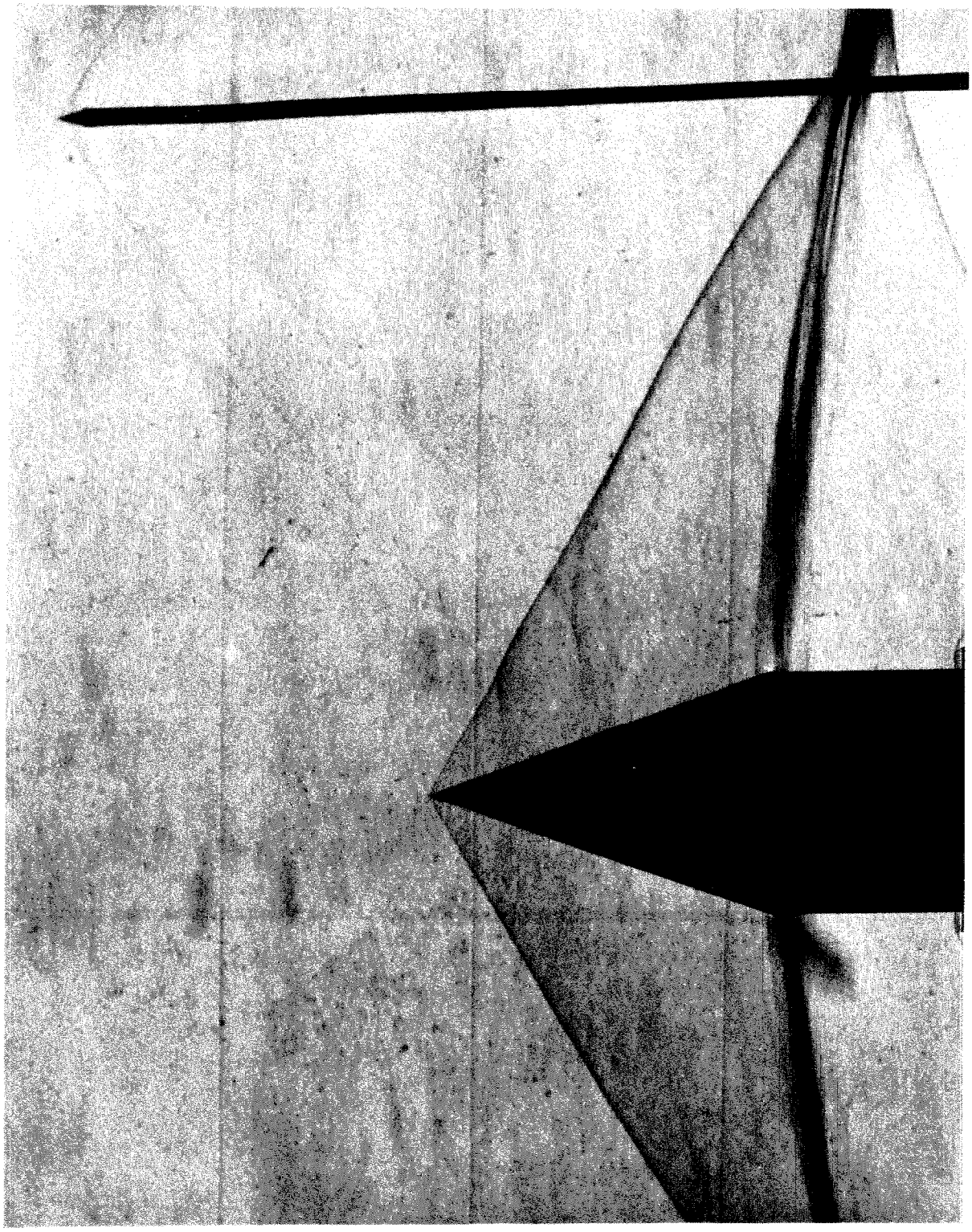

WAVE REFLECTION FROM SONIC LINE
20° SEMI-ANGLE CONE-CYLINDER
$M_\infty = 1.297$

FIG. 5

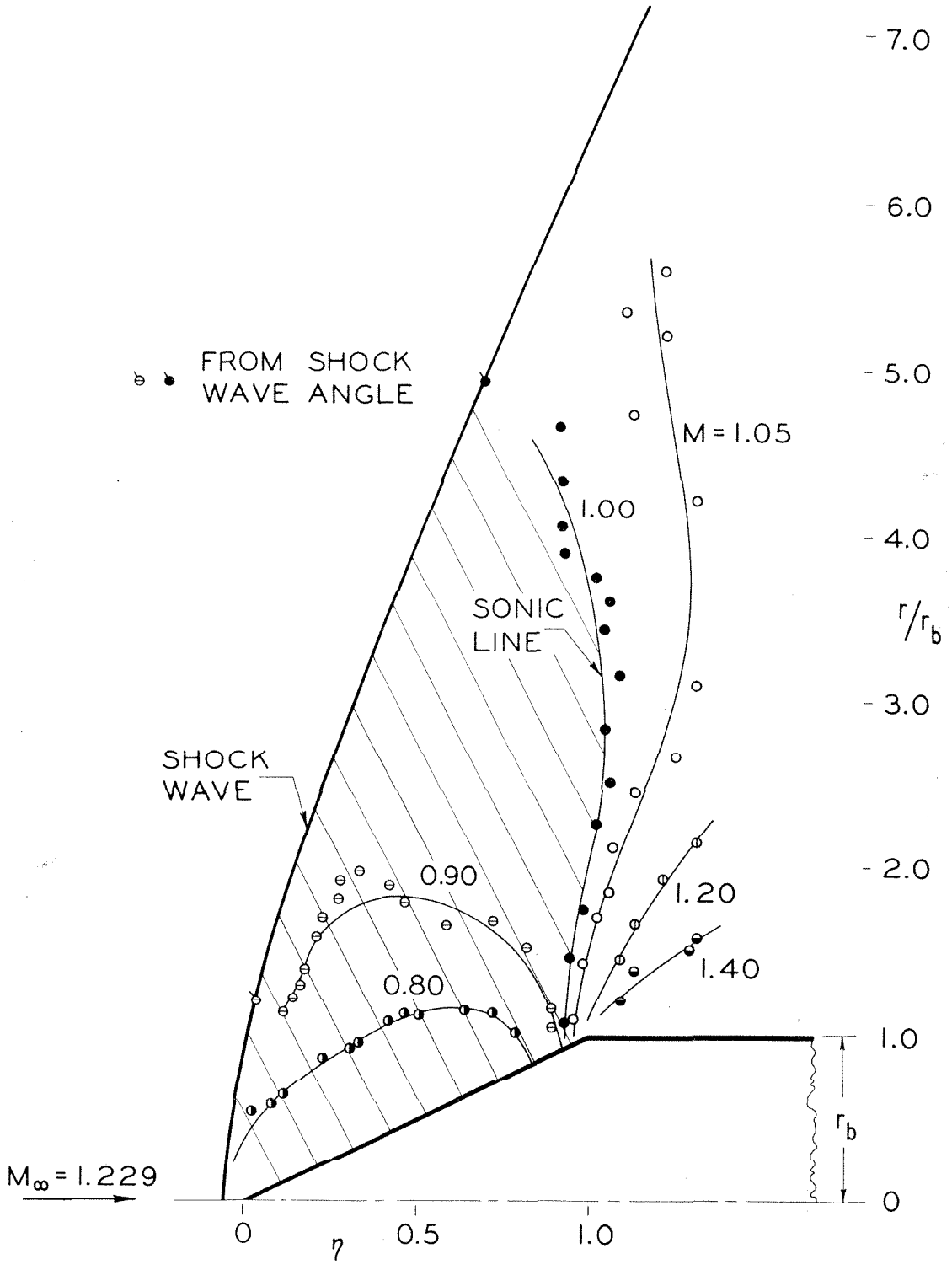

MACH NUMBER FIELD
FOR
25° SEMI - ANGLE CONE - CYLINDER

FIG. 6

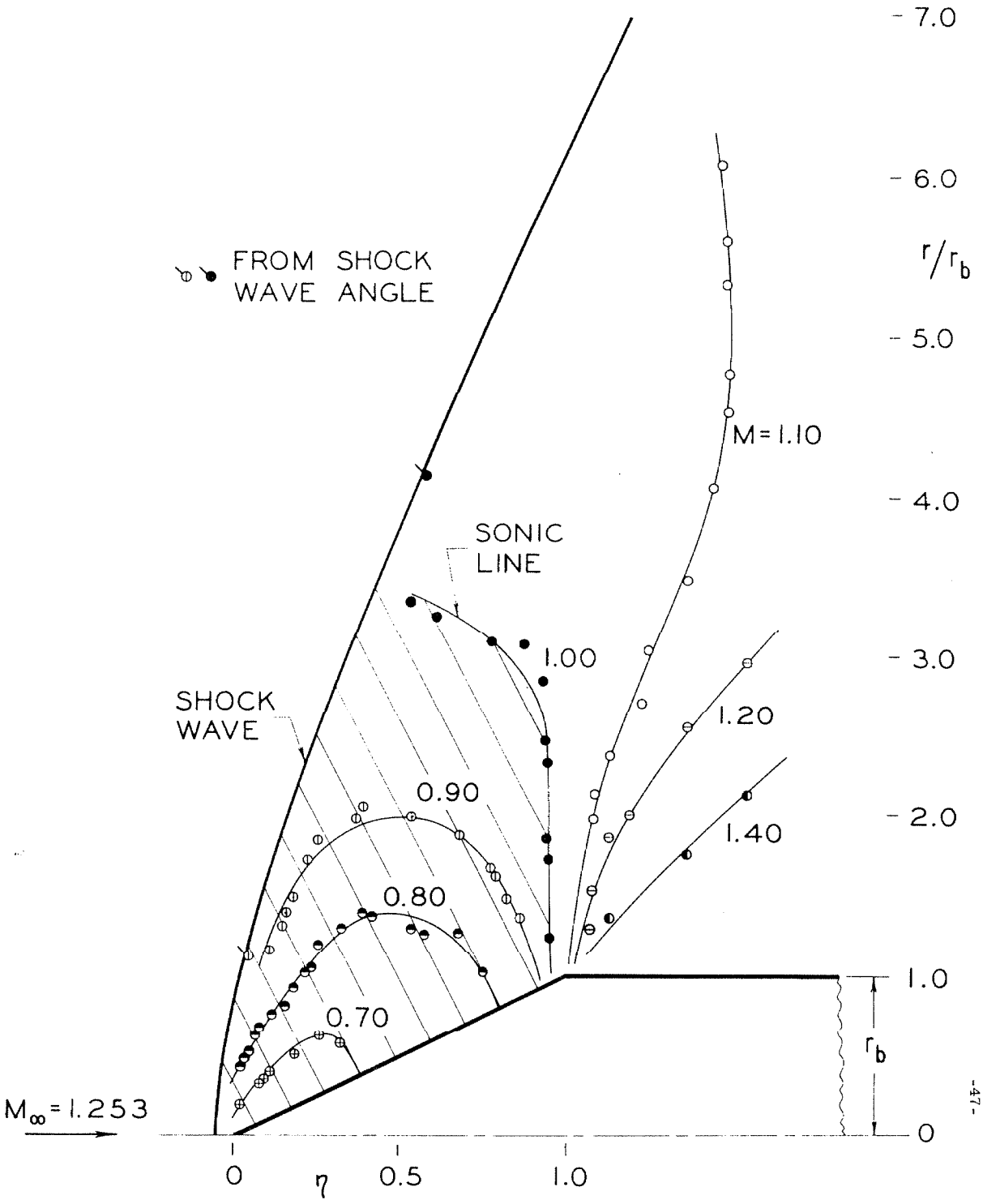

MACH NUMBER FIELD
FOR
25° SEMI-ANGLE CONE-CYLINDER

FIG. 7

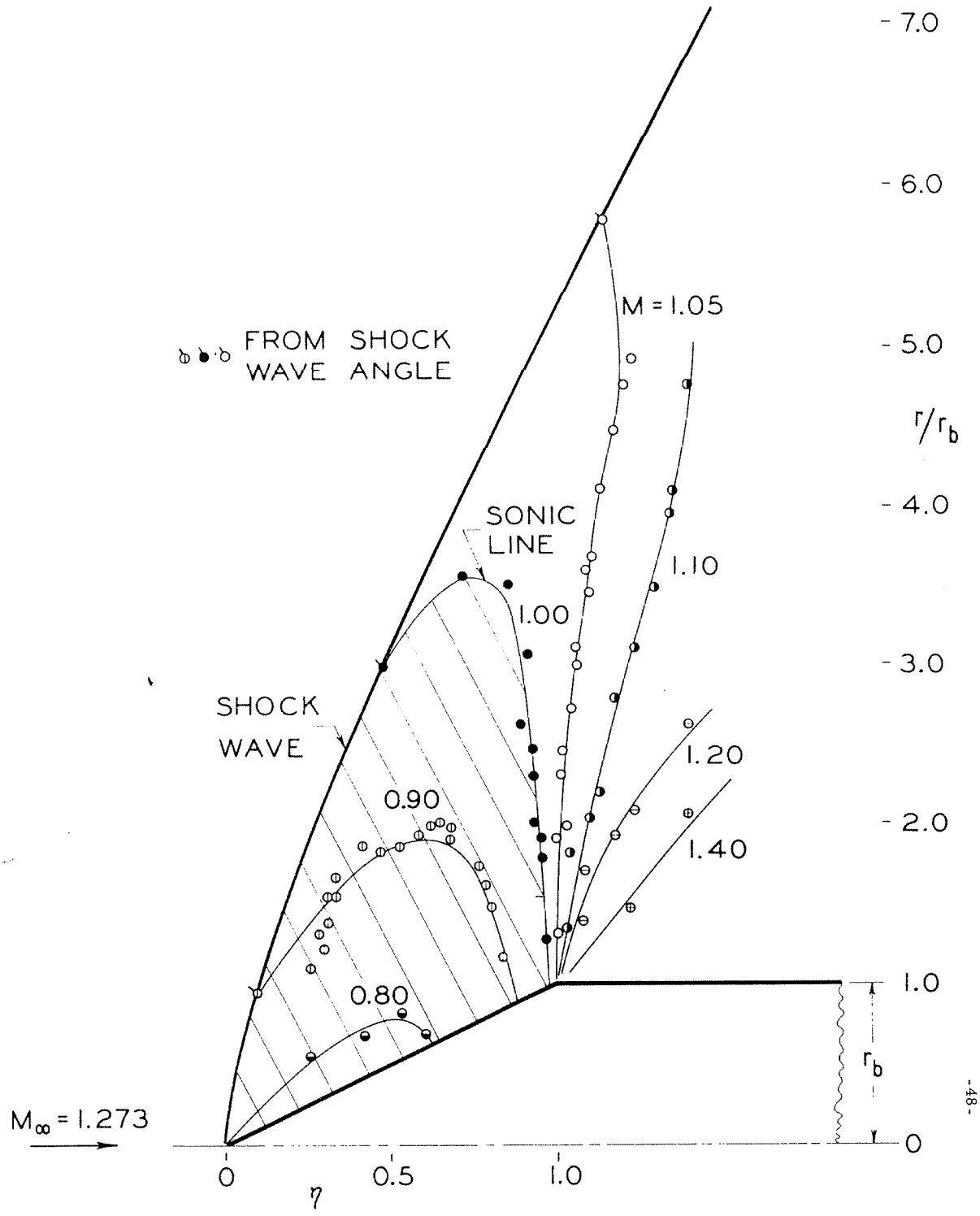

MACH NUMBER FIELD
FOR
25° SEMI-ANGLE CONE-CYLINDER

FIG. 8

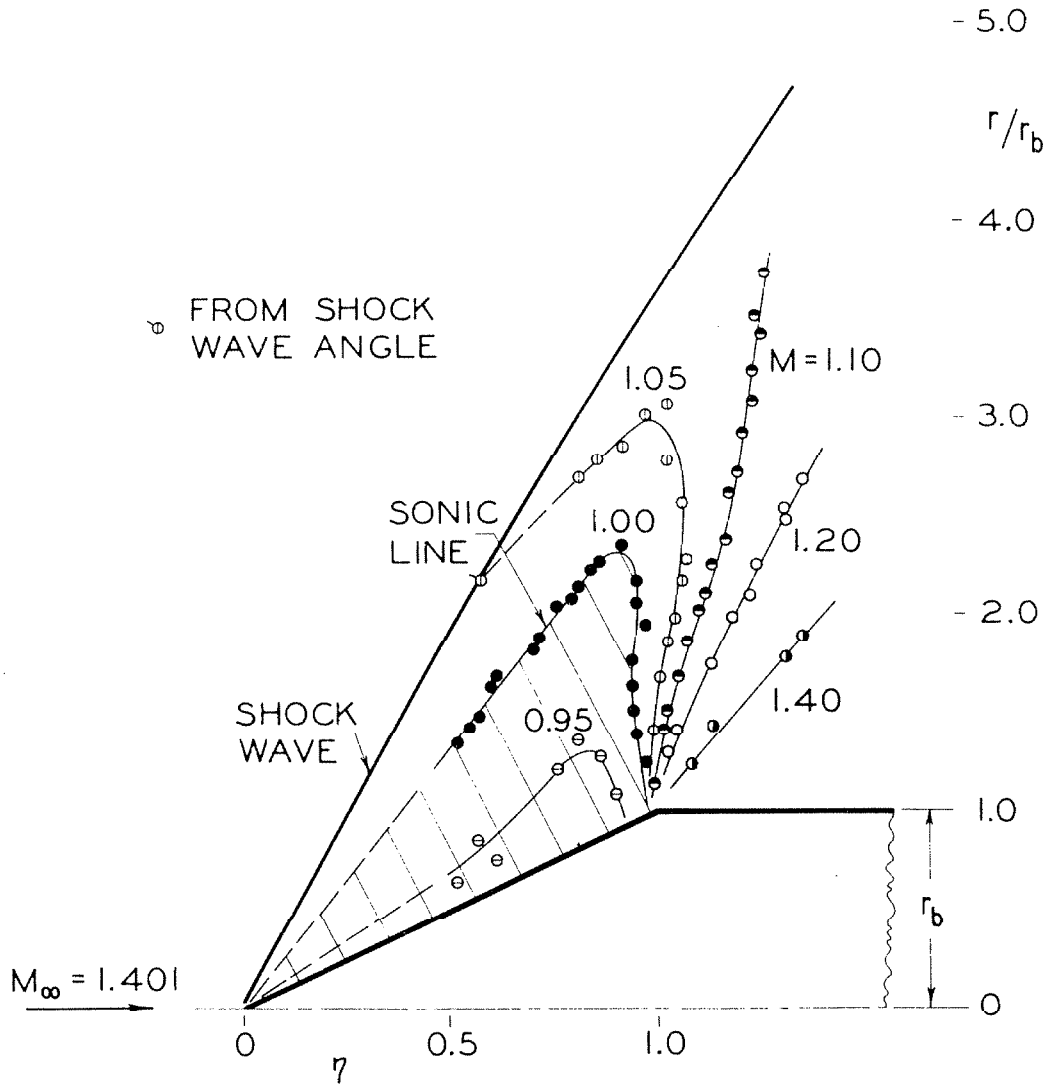

MACH NUMBER FIELD

FOR

25° SEMI-ANGLE CONE-CYLINDER

FIG. 9

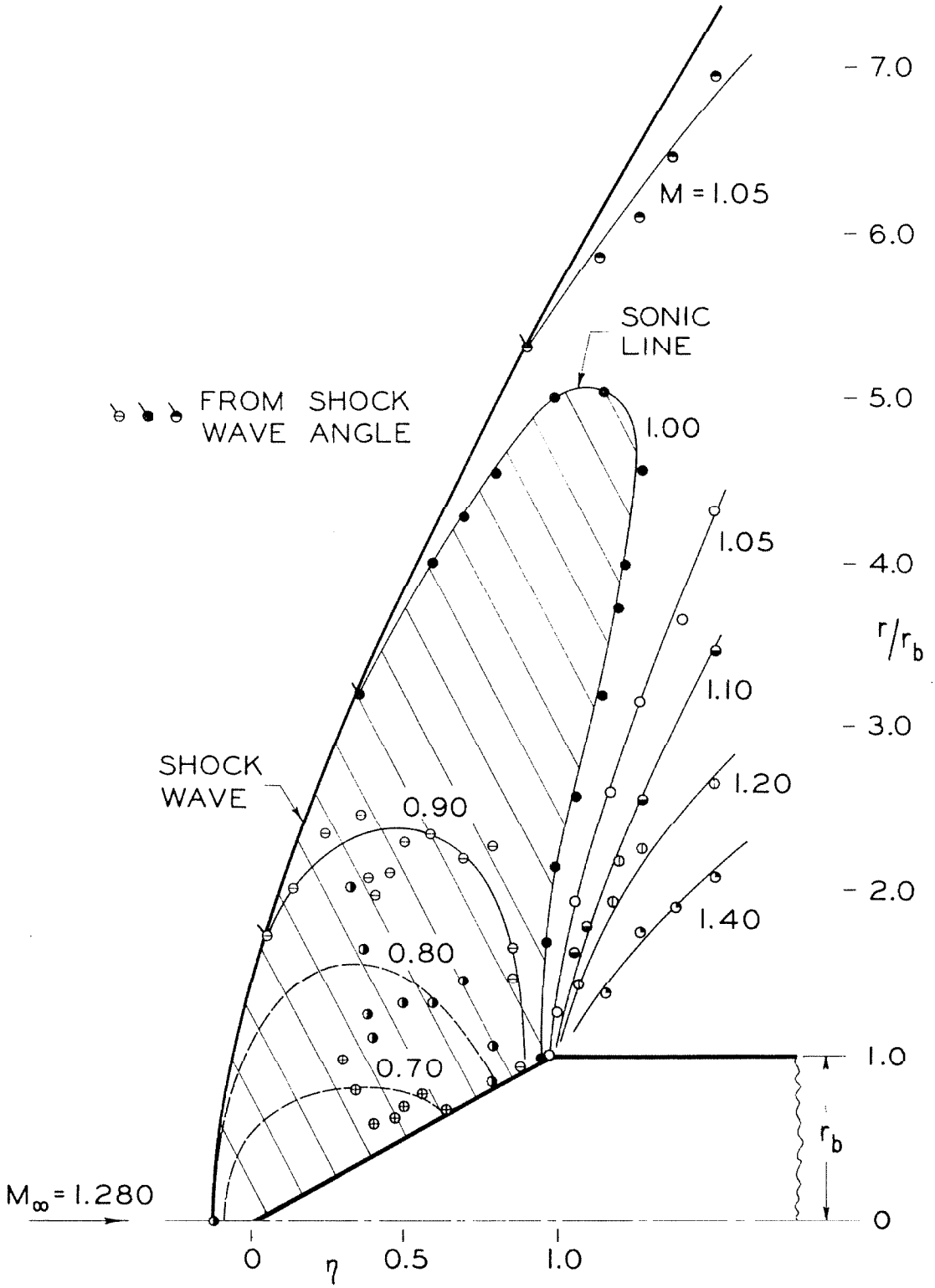

MACH NUMBER FIELD
FOR
30° SEMI-ANGLE CONE - CYLINDER

FIG. 10

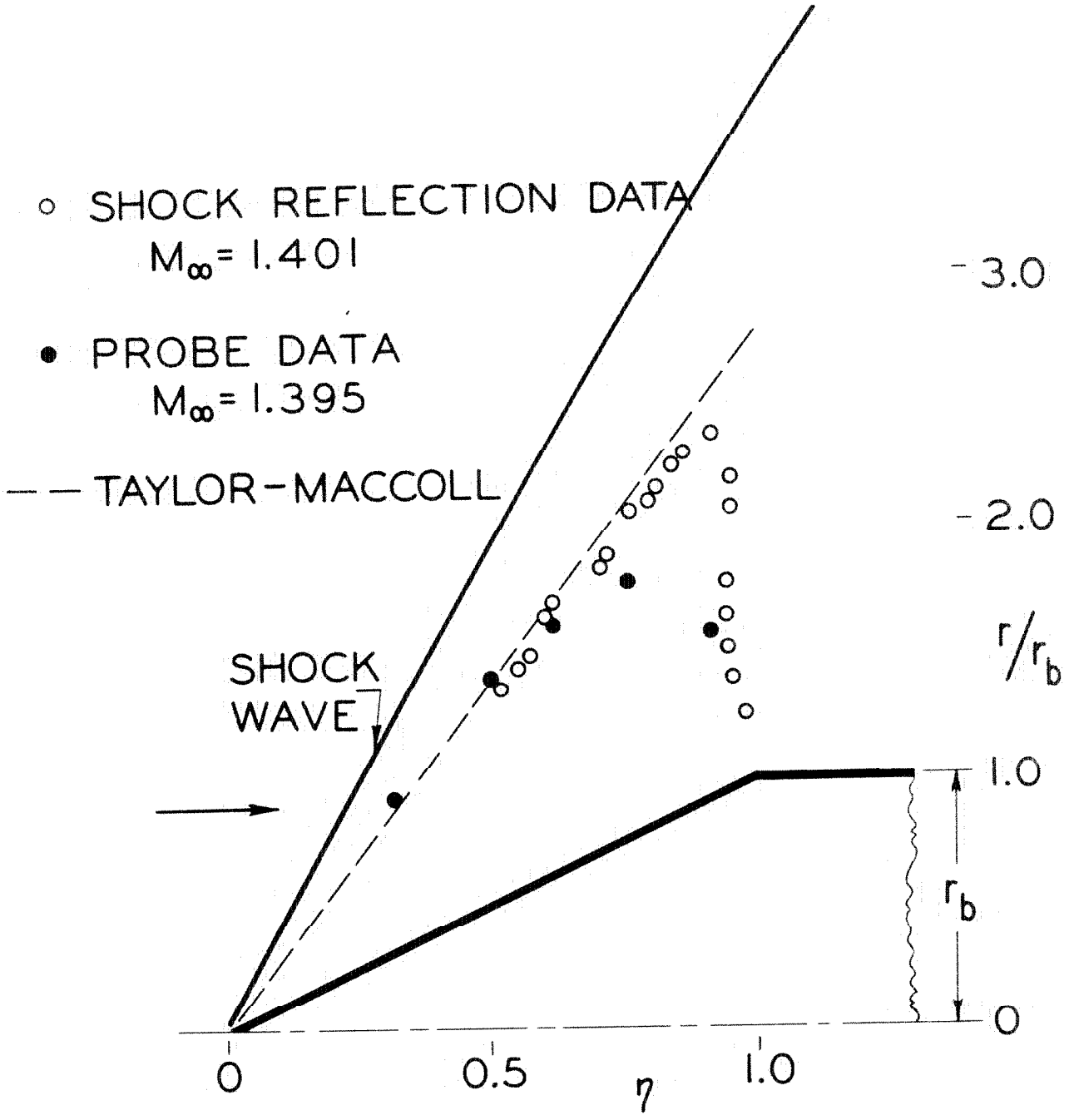

SONIC LINE LOCATION

25° SEMI-ANGLE CONE-CYLINDER

FIG. 11

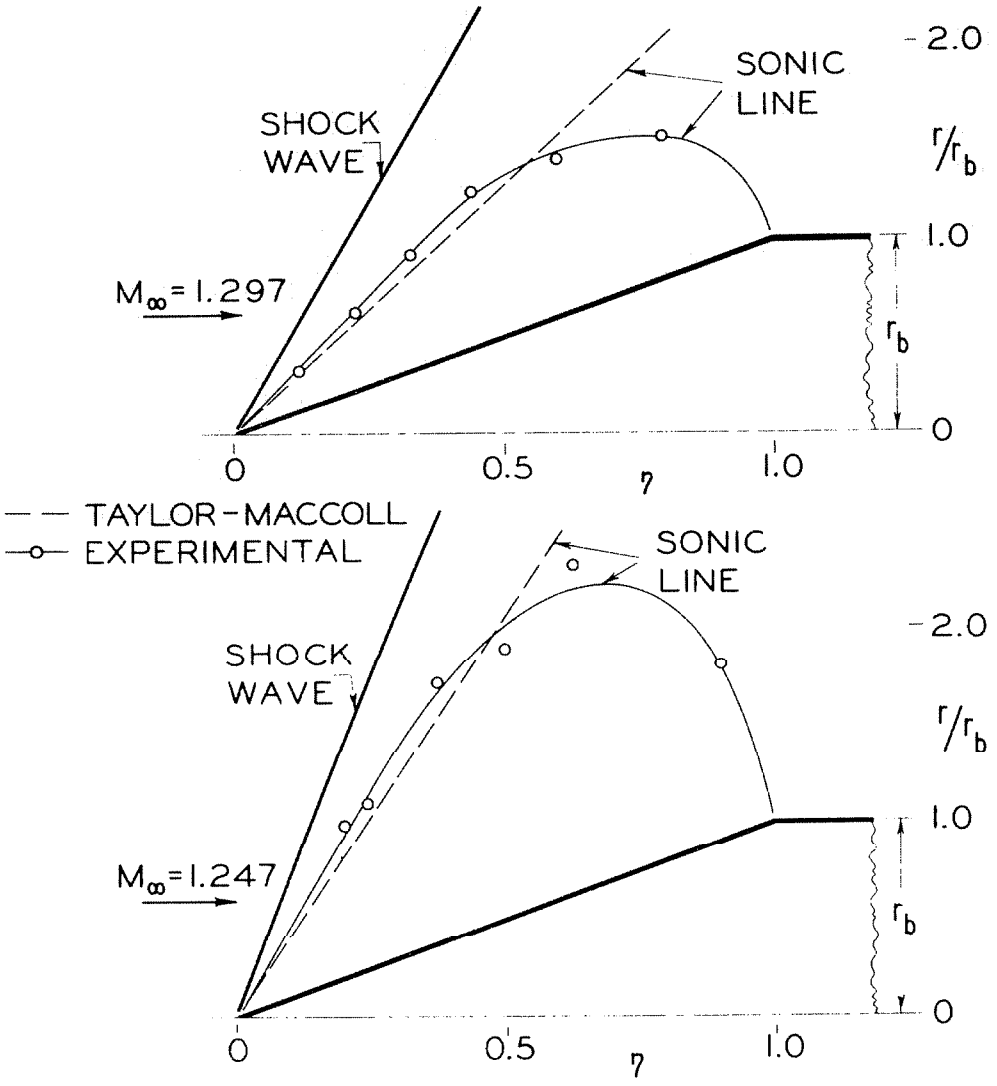

SONIC LINE LOCATION BY SHOCK REFLECTION
20° SEMI-ANGLE CONE-CYLINDER

FIG. 12

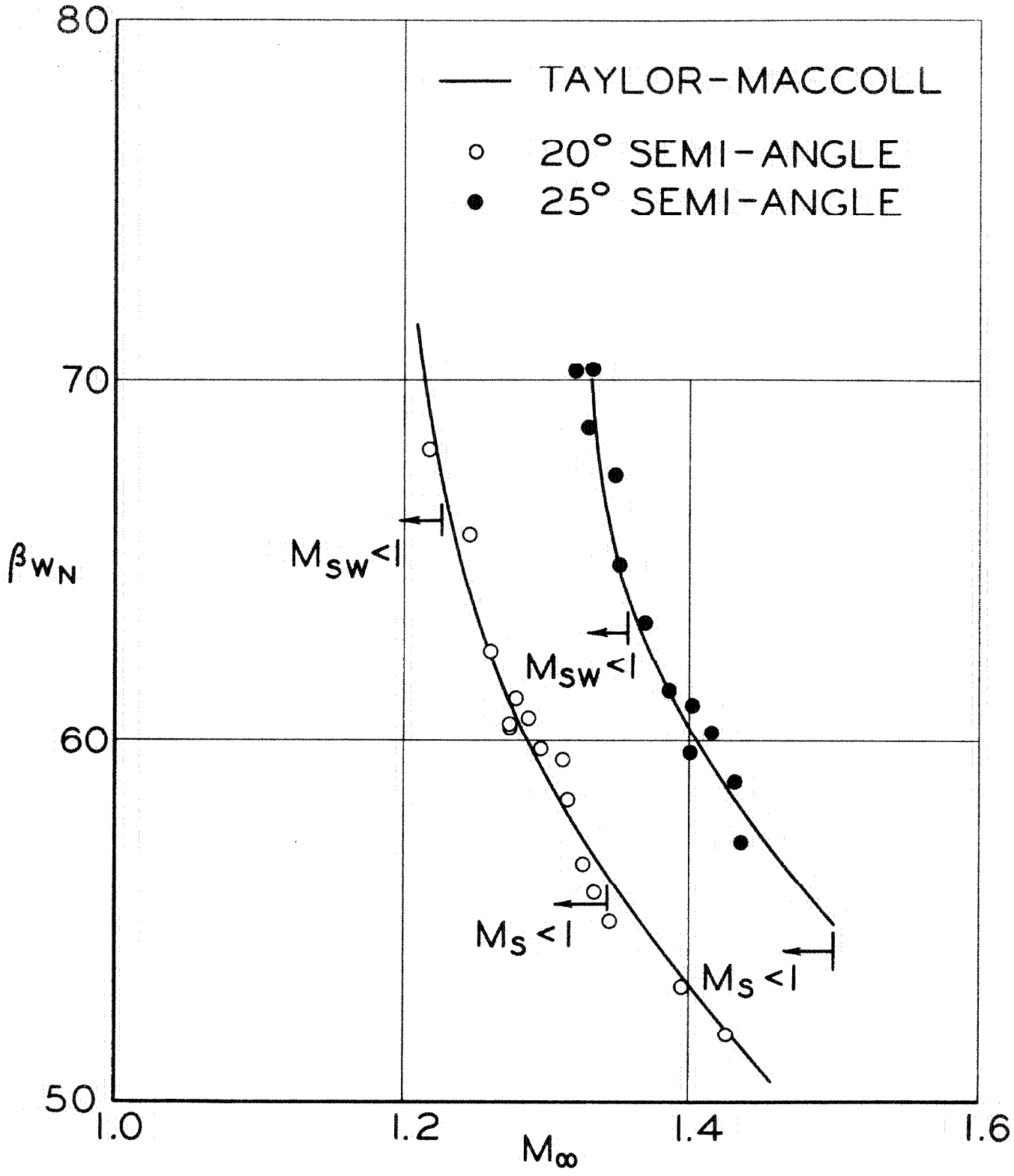

NOSE WAVE ANGLE

FIG. 13

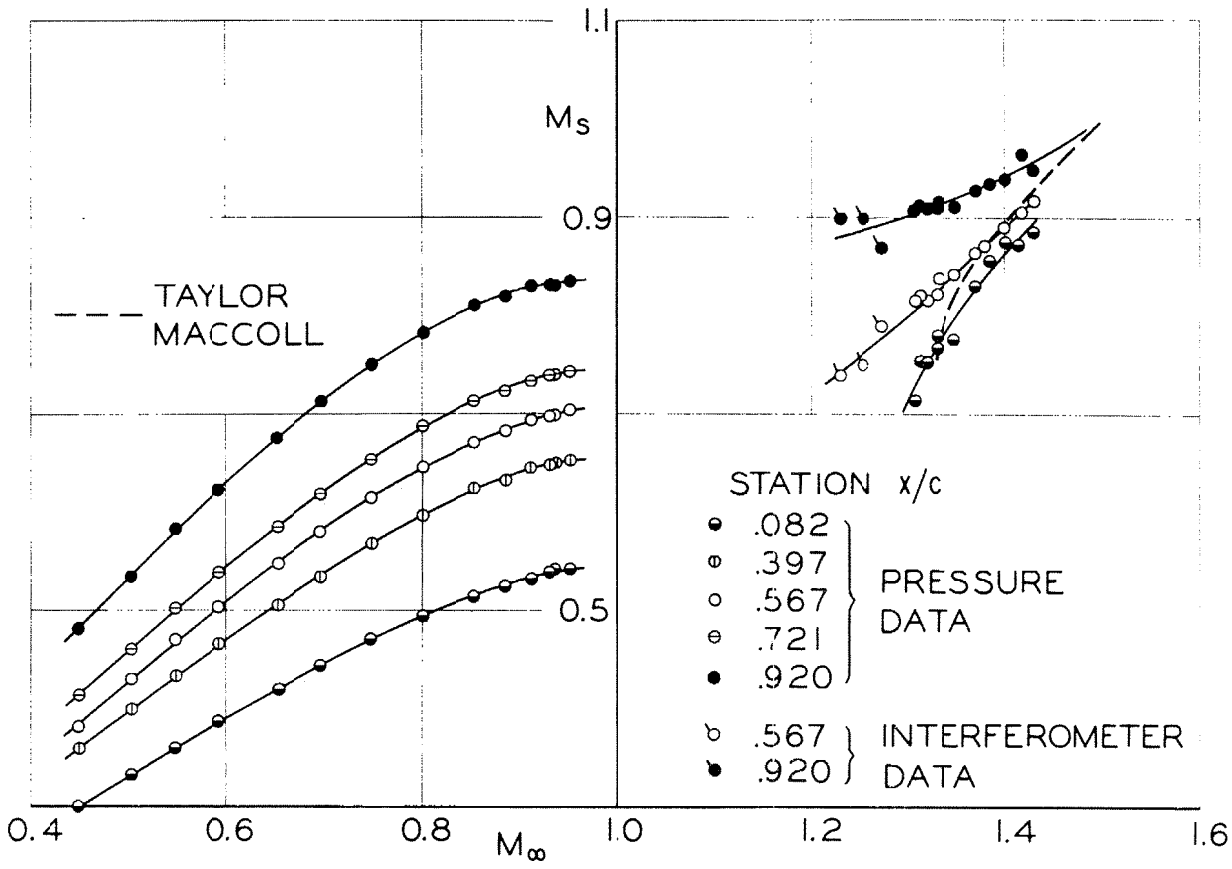

SURFACE MACH NUMBER
ON
25° SEMI-ANGLE CONE - CYLINDER

FIG. 14

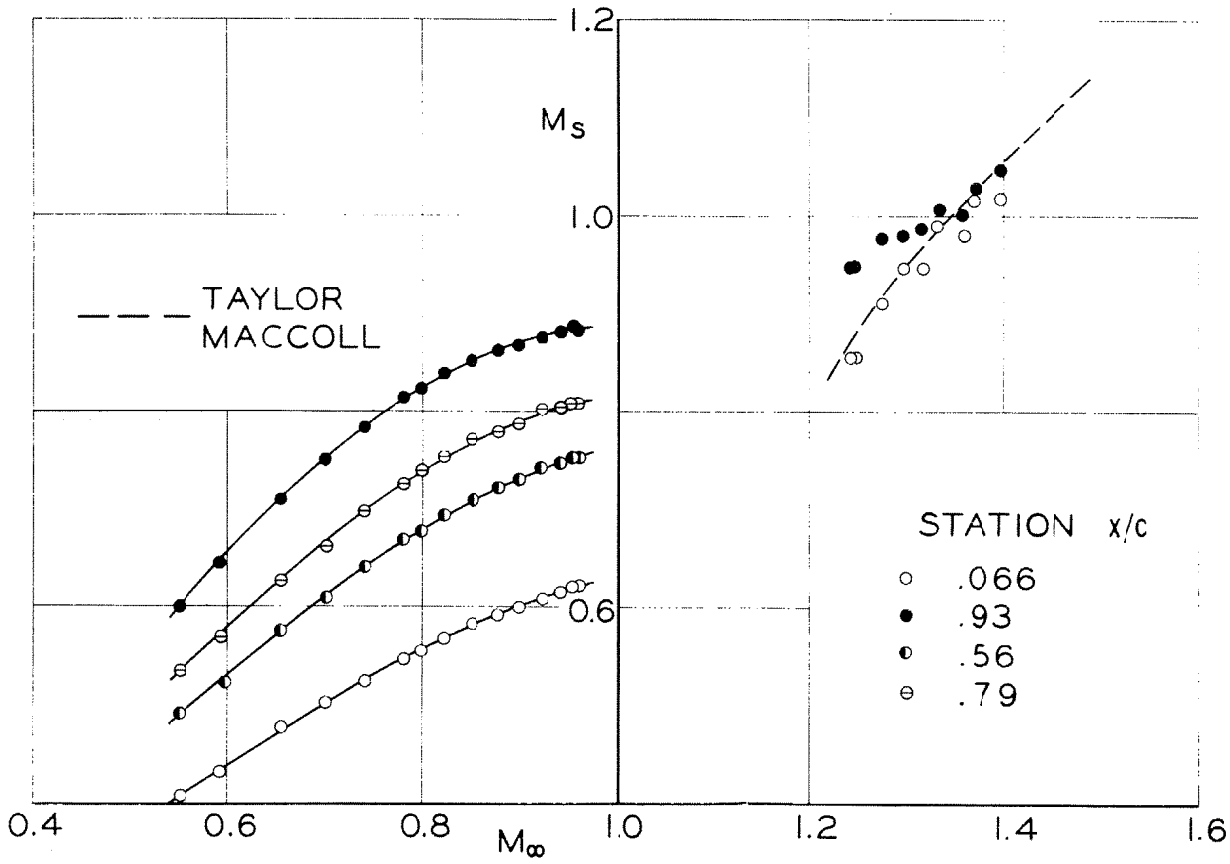

SURFACE MACH NUMBER
ON
20° SEMI-ANGLE CONE-CYLINDER

FIG. 15

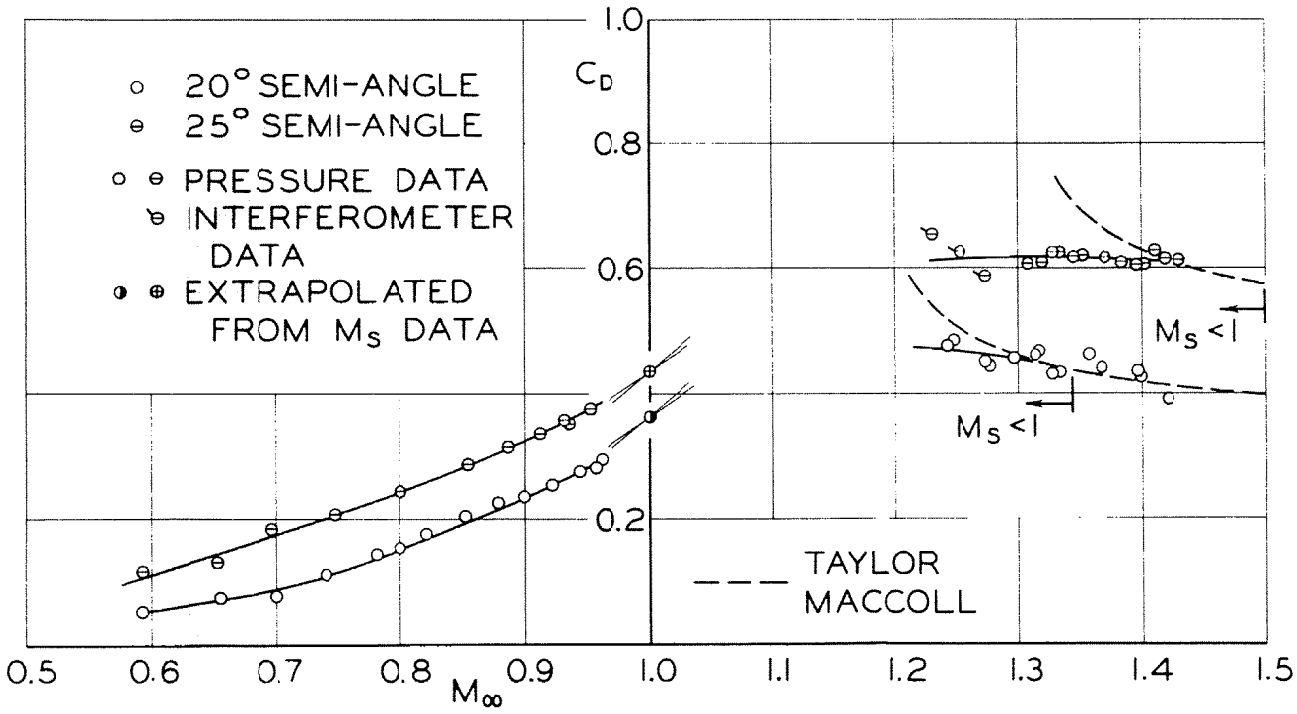

DRAG COEFFICIENTS FOR CONE-CYLINDERS

FIG. 16

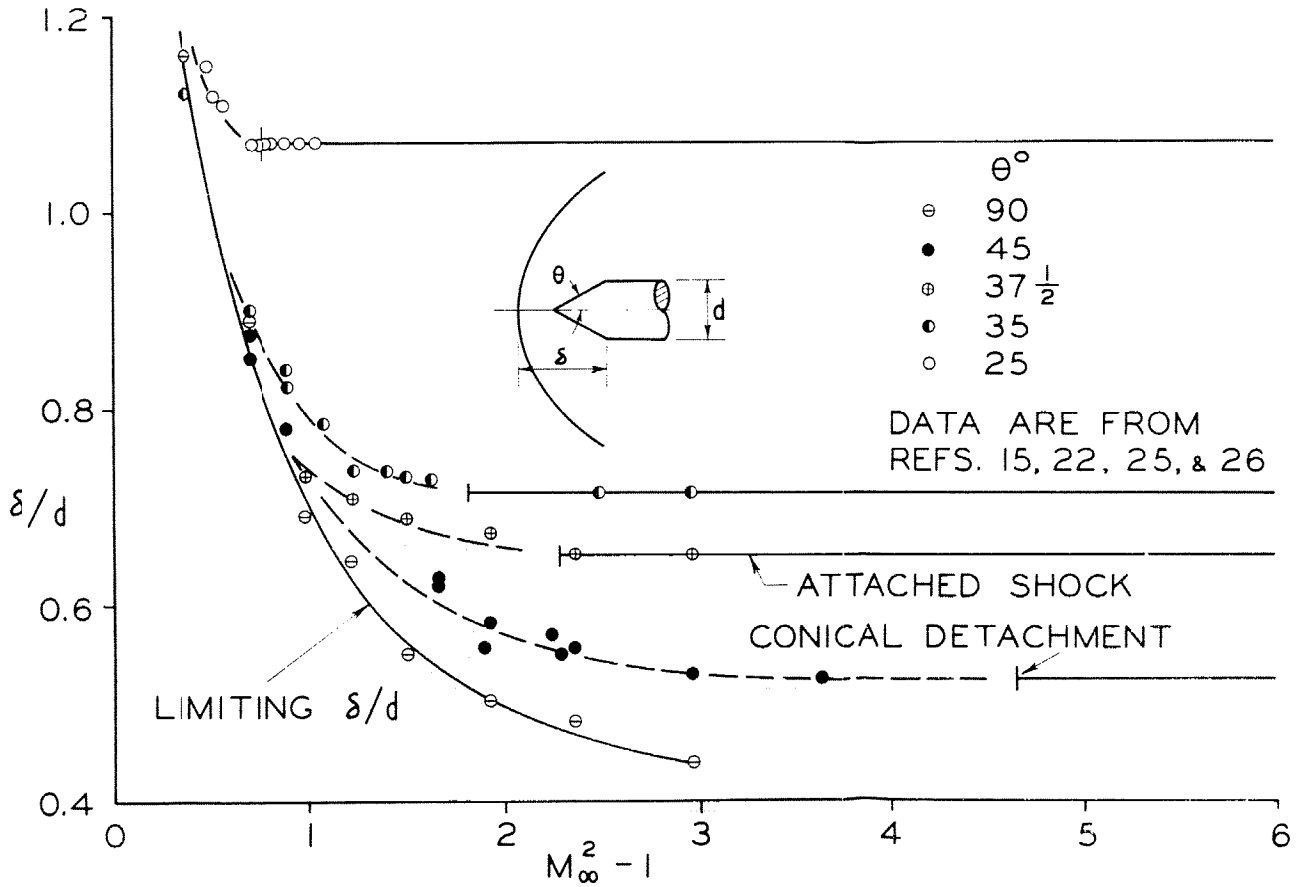

SHOCK WAVE DETACHMENT DISTANCE
FOR
FINITE CONES

FIG. 17

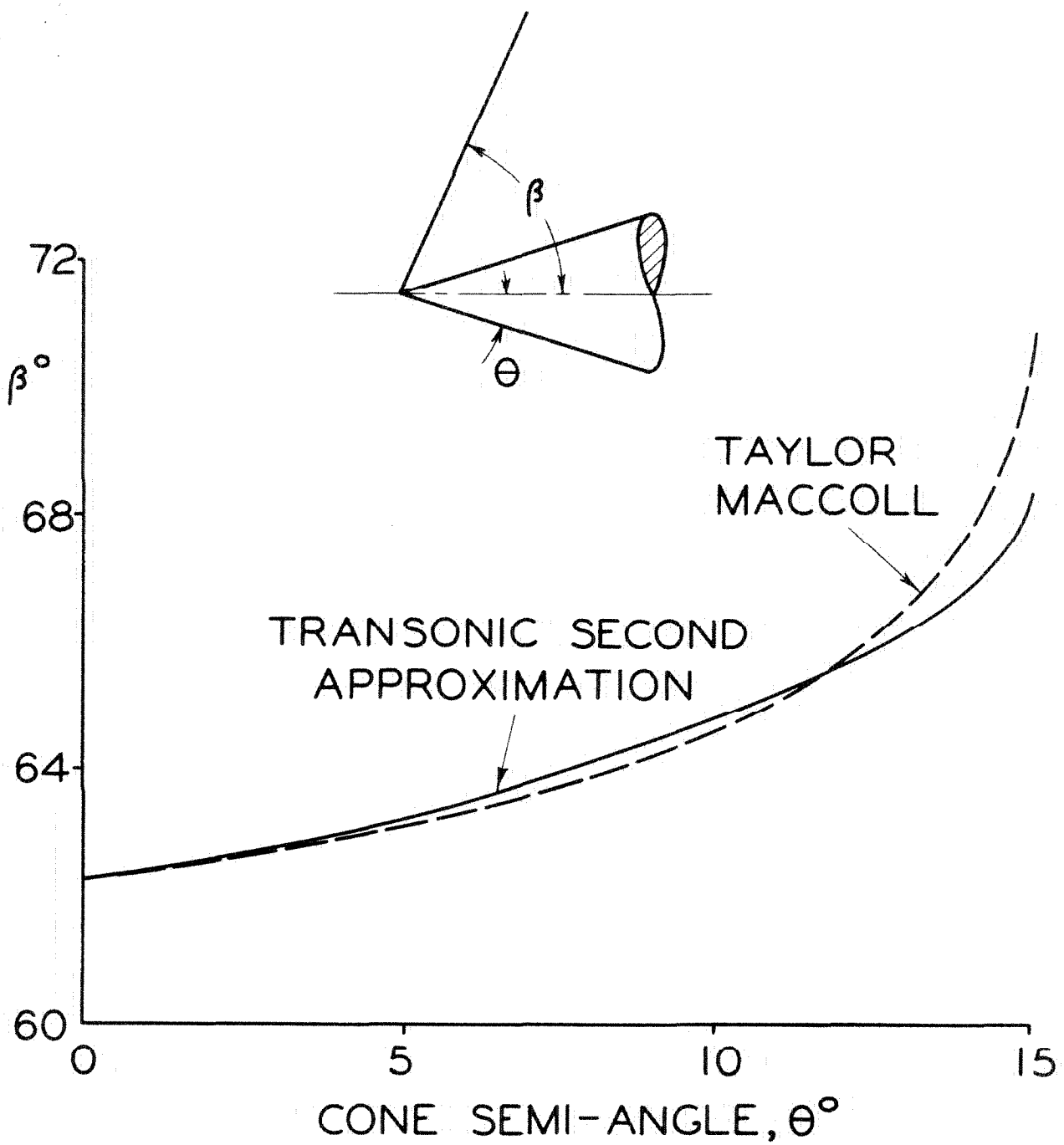

SHOCK WAVE ANGLE
FOR SEMI-INFINITE CONES
$u_\infty = 0.25$ $M_\infty = 1.12$

FIG. 18

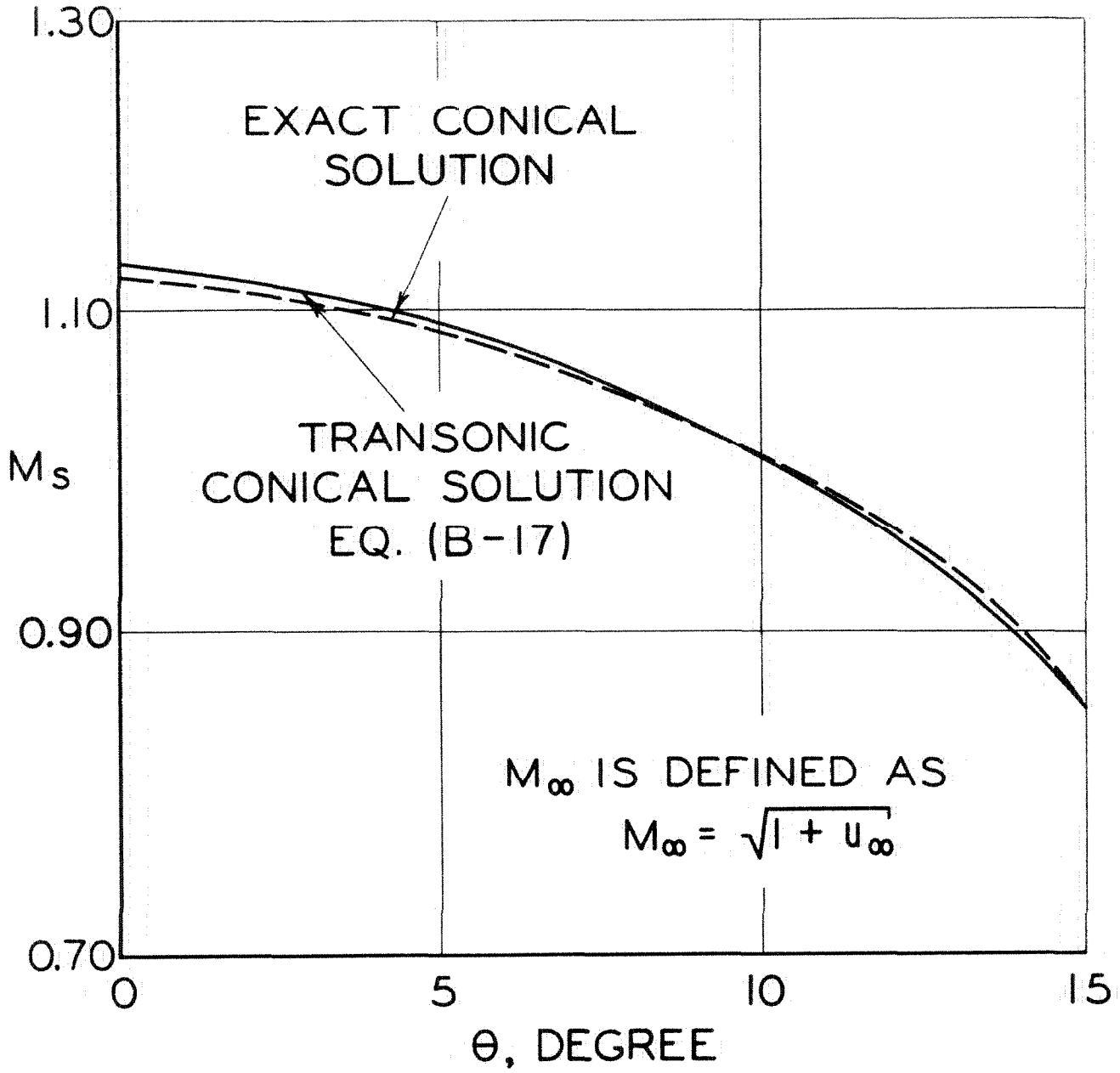

TRANSONIC CONICAL SOLUTION

SURFACE MACH NUMBER vs. CONE SEMI-ANGLE

$u_\infty = 0.25$ $M_\infty = 1.12$

FIG. 19

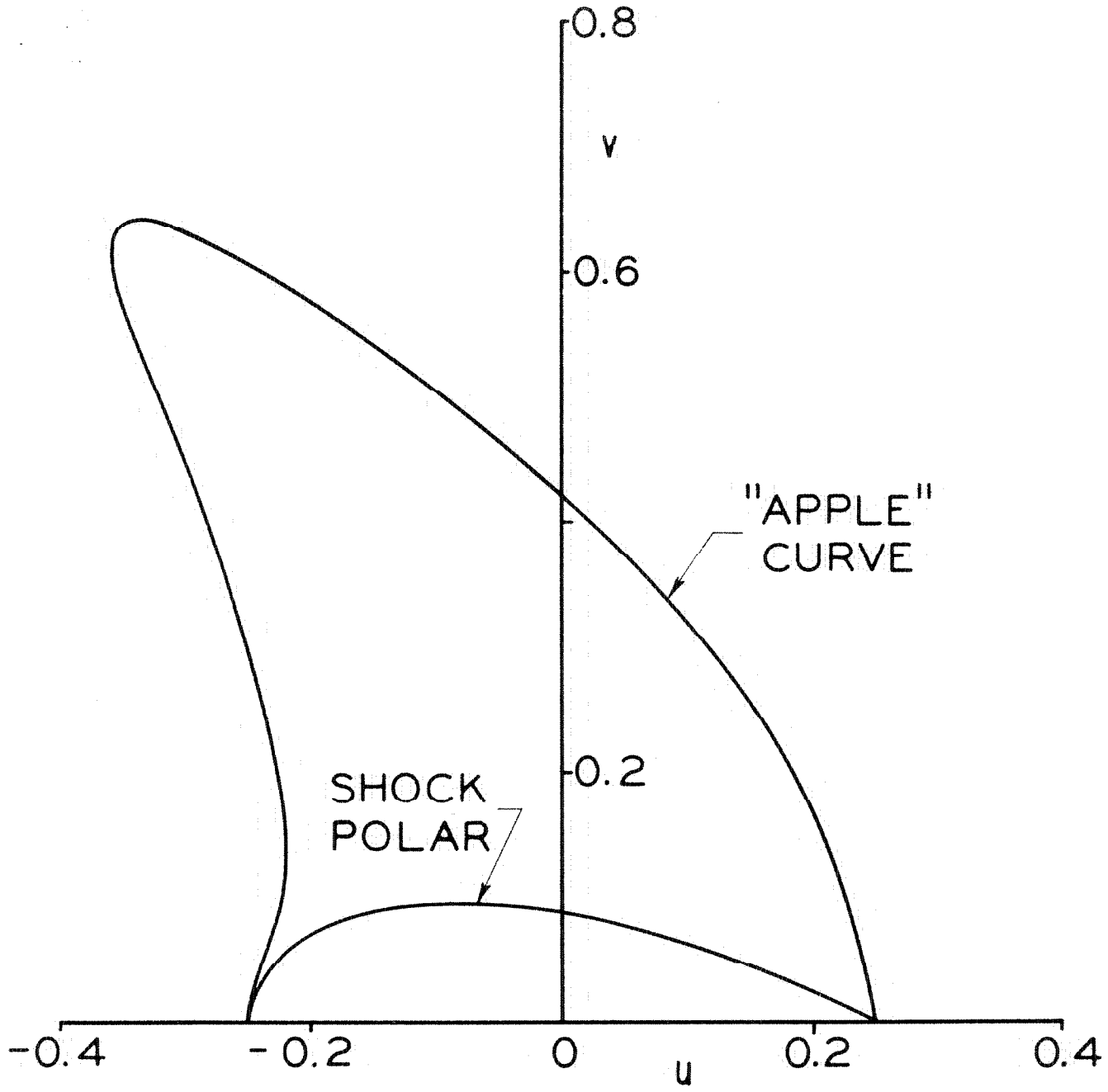

TRANSONIC "APPLE" CURVE AT $u_\infty = 0.25$
FROM SECOND APPROXIMATION

FIG. 20

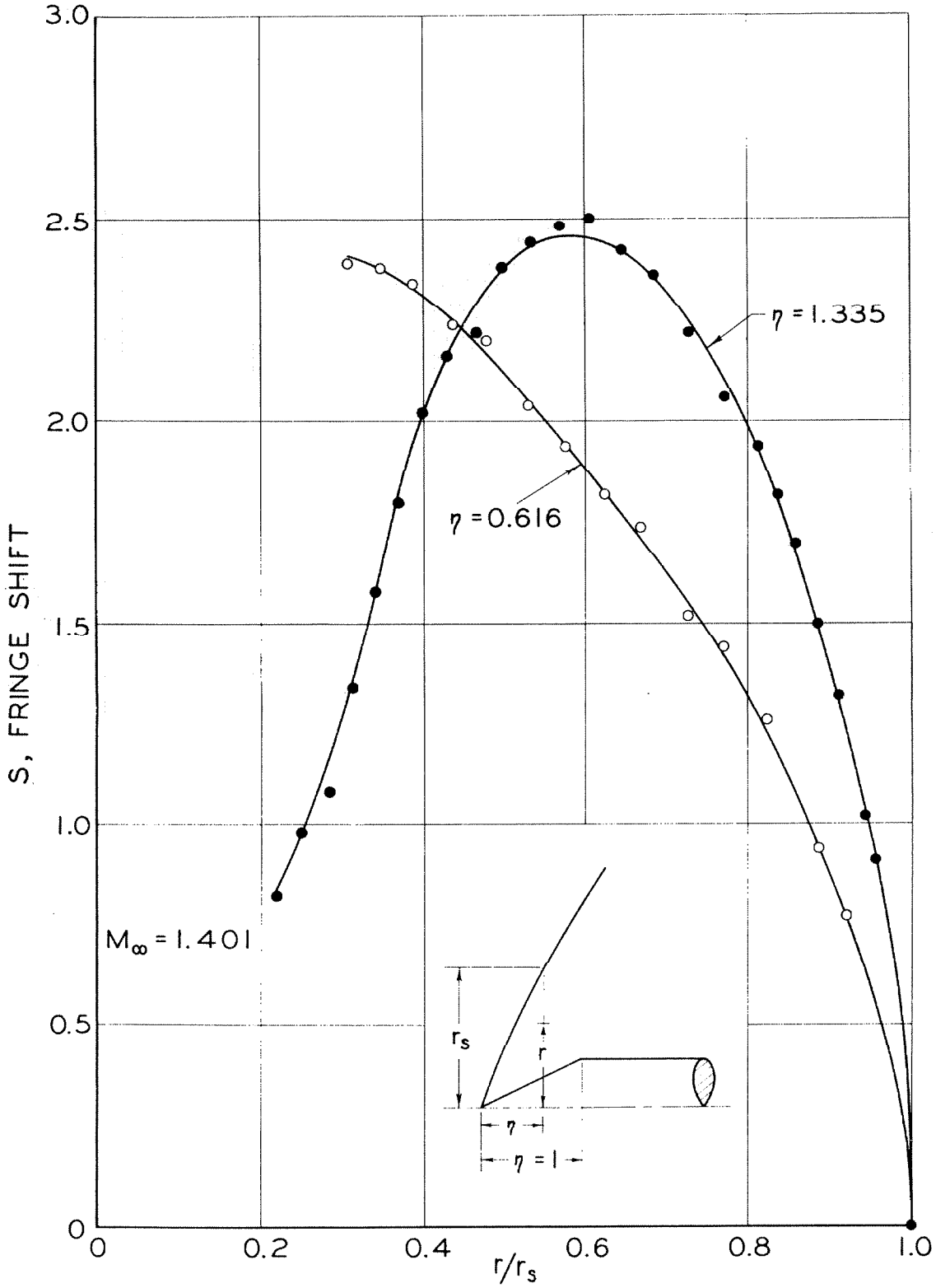

INTERFEROGRAM FRINGE SHIFTS
FOR
25° SEMI-ANGLE CONE-CYLINDER

FIG. 21